UNIVERSITY OF OKLAHOMA

GRADUATE COLLEGE

CORRELATING DELIVERABILITY TO LITHOLOGY, FAULTS, FRACTURES AND CLEATS IN COALBED METHANE EXPLOITATION

A THESIS

SUBMITTED TO THE GRADUATE FACULTY

In partial fulfillment of the requirement for the

Degree of

MASTER OF SCIENCE

By

JEREMY C. FISK

Norman, Oklahoma

2010

Acknowledgements

I would like to thank Santos, Ltd. for data for this study, technical guidance, and permission to publish this work. I thank Schlumberger for providing licenses to Petrel and CGG-Veritas for providing licenses to Hampson-Russell software for use in research and education at the University of Oklahoma.

I would like to thank my committee for teaching and training me during this project, especially my advisor Kurt Marfurt. Kurt was a great friend, great boss, and his industry-focused research allows students to gain important exposure to the business world. Additionally, I deeply appreciate the mentorship of Dr. Carl Sondergeld. I would also like to thank Marcilio Matos, Mike Burnett, John Hooper and Tim Kwiatkowski for all their assistance in this project. I would like to thank my fellow students that helped me in some way on this project to include Sunday Amoyedo, Oz Elis, Bryce Jensen, Ha Mai, Shamik Bose, Brad Wallet, Oswaldo Davogussto, Kui Zhang, Roderick Perez, and Nabanita Gupta. Finally, I would like to thank my wife, Britt, for her support.

Table of contents

List of figures

Abstract

Similar to other unconventional reservoirs, coalbed-methane reservoirs have sweet spots that are a function of fracture density, fracture connectivity, rank, and storage capacity. Coalbed-methane reservoirs can be financially lucrative because of the shallow optimal depth windows at which they are usually found (500 - 5,000 ft) and their tendency to display more gradual decline curves than conventional wells. These reservoirs are quite complex, such that successful exploitation of these reservoirs requires consideration of a number of important variables. Successful horizontal drilling in these reservoirs depends on the operator's ability to identify face cleat directions and drill perpendicular to the face cleat. Seismic curvature attributes, azimuthally sorted seismic data, and acoustic impedance inversion can be applied in such a way to provide added insight to the cleat directions in coalbed-methane reservoirs.

Australia is the world's second largest producer of coalbed-methane. Characterized as a marginal tectonic setting, the Bowen Basin of Queensland displays a thick succession of numerous thin (1.2-11.0 m) bituminous-rank coal seams. The area's heterogeneous gas production is particularly perplexing; it is not unusual for production to change as much as 50-75% between neighboring wells within a few kilometers of one another. A myriad of factors can affect coalbed-methane production including coal rank, coal thickness, coal cleat architecture, ash content, mineralization of fractures in the coal, the local maximum horizontal stress direction, and the *in situ* stress magnitude.

Seismic curvature attributes illustrate lineaments that correlate to production. Most-positive principal structural curvature lineaments in the direction perpendicular to the maximum horizontal stress revealed areas of lower gas rates for nearby wells. High amplitude curvature lineaments intersect the wellbore of a high producing well along the azimuths of maximum and minimum horizontal stress. High acoustic impedance amplitude curvature lineaments are more prevalent in areas of low gas production and weaker acoustic impedance lineaments are present in areas of high gas production. I use a technique to generate 3D rose diagrams from curvature attributes and show that the diagrams depict the face and butt cleat architecture. Areas with bi-directional, orthogonal rose diagrams had higher gas rates and reflect the existence of both sets of cleats. I explain the benefits of low density coal in a reservoir and apply multiattribute transforms to generate predictive prospectivity volumes for reservoir rock properties such as density. In this region, I found that low density coal frequently corresponds with dome and ridge features. Furthermore, zones of high flexure, such as areas with dome features, possess low acoustic impedances that are an expression of locations of low density, low velocity open cleats and fractures. In this coalbed-methane reservoir, the operator found image logs uncover small scale permeability barriers such as shale streaks and mineral-filled cleats and fractures. Finally, stacked azimuthal gathers provide evidence of face cleat direction by illustrating areas of high acoustic impedance related to fast directions of travel for P-wave velocities.

I. Introduction

Unconventional reservoirs continue to contribute an increasing percentage of the total amount of oil and gas production in the world. Shale and coal are examples of low-permeability unconventional reservoirs that often act as both the primary source and reservoir rock. The limitations of seismic resolution are often a point of discussion among geoscientists seeking to characterize these unconventional reservoirs. Slatt (2006) likens this problem to a seismic wavelet being superimposed on a building, whereby the building is resolved by the wavelet, but the individual rooms, floors, ceilings and walls (e.g., reservoir compartments) cannot be imaged because they are beneath seismic resolution. Nevertheless, the application of seismic attributes, multiattribute transforms and spectral decomposition enhance subtle features in the seismic data thereby facilitating a more detailed reservoir characterization.

Geophysicists have conducted numerous studies relating the seismic response of coal, coal cleats, and coal fractures to methane production. Marroquin and Hart (2004) correlate lineaments seen in seismic attributes to production in coals in the Fruitland Formation. McCrank and Lawton (2009) present a seismic study that includes seismic horizon interpretations and an acoustic impedance inversion of Ardley coals in Canada. Chopra et al. (2009) combine curvature, azimuth, and shape attributes to generate 3D rose diagrams that are correlated to fractures seen in image logs as well as production. In addition, Ramos and Davis (1997) apply amplitude versus offset (AVO) analysis to 3D seismic data of Cedar Hill Field, New Mexico and relate fracture densities in coals to Poisson's ratio contrasts.

Multiattribute transforms allow interpreters to marry seismic data with rock properties from well logs in reservoirs such as coal seams. Hampson et al. (2001) summarize how to construct multiattribute transforms to predict log properties from seismic data through two case studies. Pramanik et al. (2004) use geostatistics and multiattribute transforms to predict porosity in thin clastic reservoirs containing coal and shale layers. Marroquin and Hart (2004) apply multiattribute analysis to map coal thicknesses in the Fruitland Formation.

I begin by reviewing the geologic background of the Bowen Basin and the basics of coalbed-methane reservoirs. Next, I review the seismic data quality. I then use multiattribute transform techniques to identify the characteristics of higher-producing coal lithologies. Finally, I relate seismic attributes and well logs to enhanced fracture permeability in the coals.

II. Geological Background

The Bowen Basin is a Permian-Triassic age major economic coal basin that extends approximately 900 km in a generally north to south direction in the eastern portion of Queensland, Australia. The Bowen Basin is one portion of the Bowen-Gunnedah-Sydney foreland system that formed as a result of the collision of the paleo-Pacific and paleo-Australian plates beginning as early as 294 Ma in the Early Permian. This orogenic belt is often referred to as the New England fold belt. The foreland system overlays a basement of volcanic and marine sedimentary rocks from the Silurian through the Carboniferous (Pattison et al.,1996). Figure 1 is a map of Australia which outlines the approximate geographical limits of the Bowen Basin in Queensland.

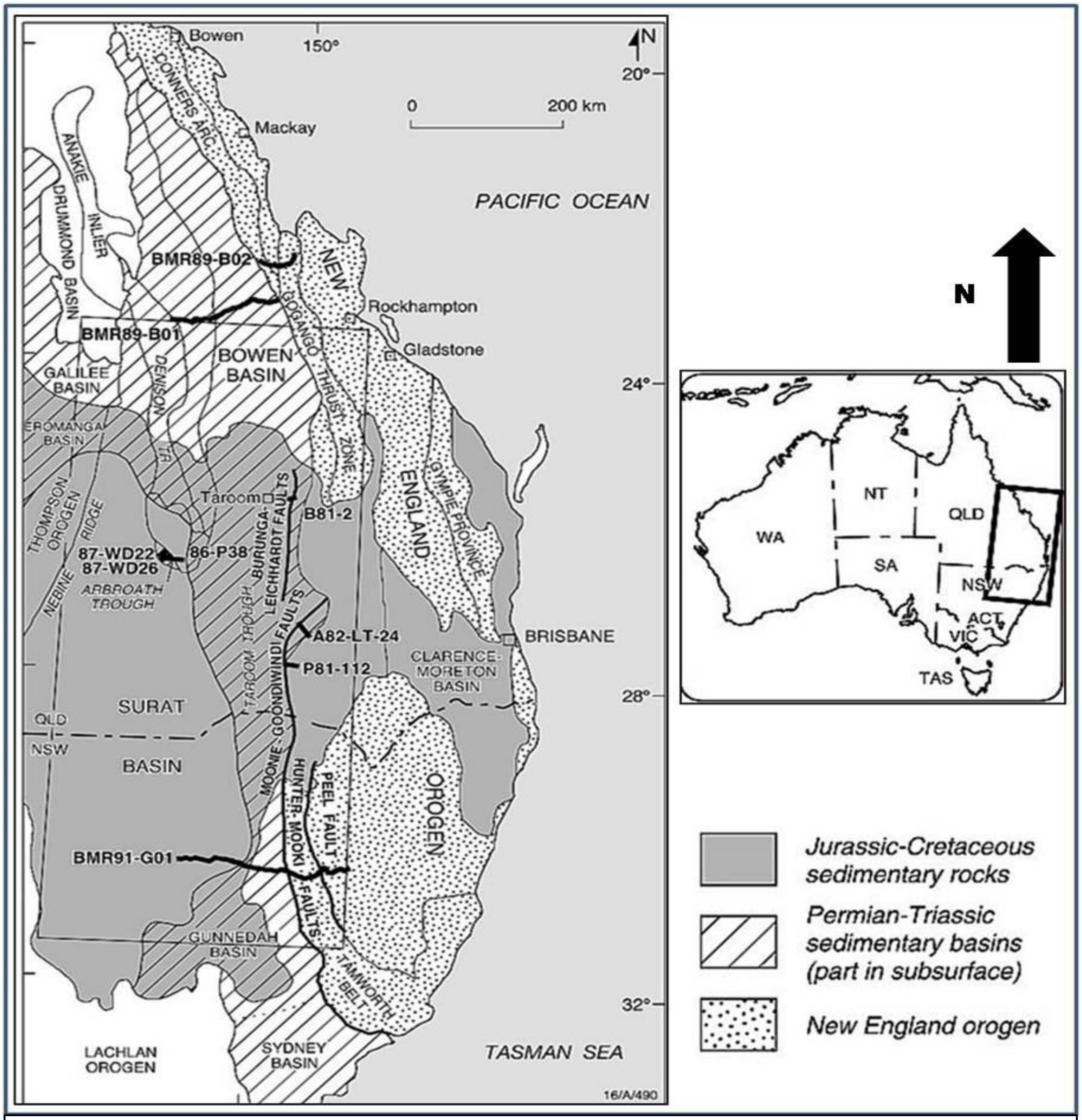

Figure 1. Geology of eastern Australia showing the Bowen and Surat Basins. In addition to extensive coal deposits, the Bowen and Surat Basins contain more than 70 small commercial oil and gas fields. Many of these fields are in anticlines that formed due to the New England orogen thrusting (Korsch, 2004).

Due to its location next to the cratonic platform, the Bowen Basin is considered to be a marginal basin. Deep troughs in the eastern side of the basin are associated with the New England orogen thrusting and crustal thickening, and were subjected to high rates of subsidence in the late Permian. Toward the end of the Permian, the coal measures formed in a fluvio-deltaic environment with fluvial elements transitioning to a paludal complex. Marginal basins in Australia tend to be characterized by a thicker sequence of coals broken into numerous coal seams and generally contain a lower coal- to-sediment ratio than intracratonic basins (Hunt and Brakel, 1989).

Stratigraphically, the Middle Permian age middle coal measures lie directly below the productive coal seam reservoir and consist of moderately developed coal seams with interbedded sandstones and siltstones. Coals are often classified by their lithotypes based on the maceral composition. Scott (2002) suggests bright coals to be rich in vitrinite-group macerals and dull coals to be inertinite-rich. Figure 2 is a condensed stratigraphic column for the formations of interest in this study. The middle coal measures are dull coal measures deposited in a "low to moderate energy, fluvial, back swamp to deltaic environment" (Ostler, 2002). Conformably overlying the middle coal measures, the reservoir is composed of the Middle Permian age upper coal measures that are well developed bright coal seams displaying brittle behavior. These upper coal measures also have interbedded siltstone and sandstone that were deposited in a fluvio/deltaic low energy environment. The Rewan Group is a Triassic age thick sequence of poor to moderately sorted sandstone with

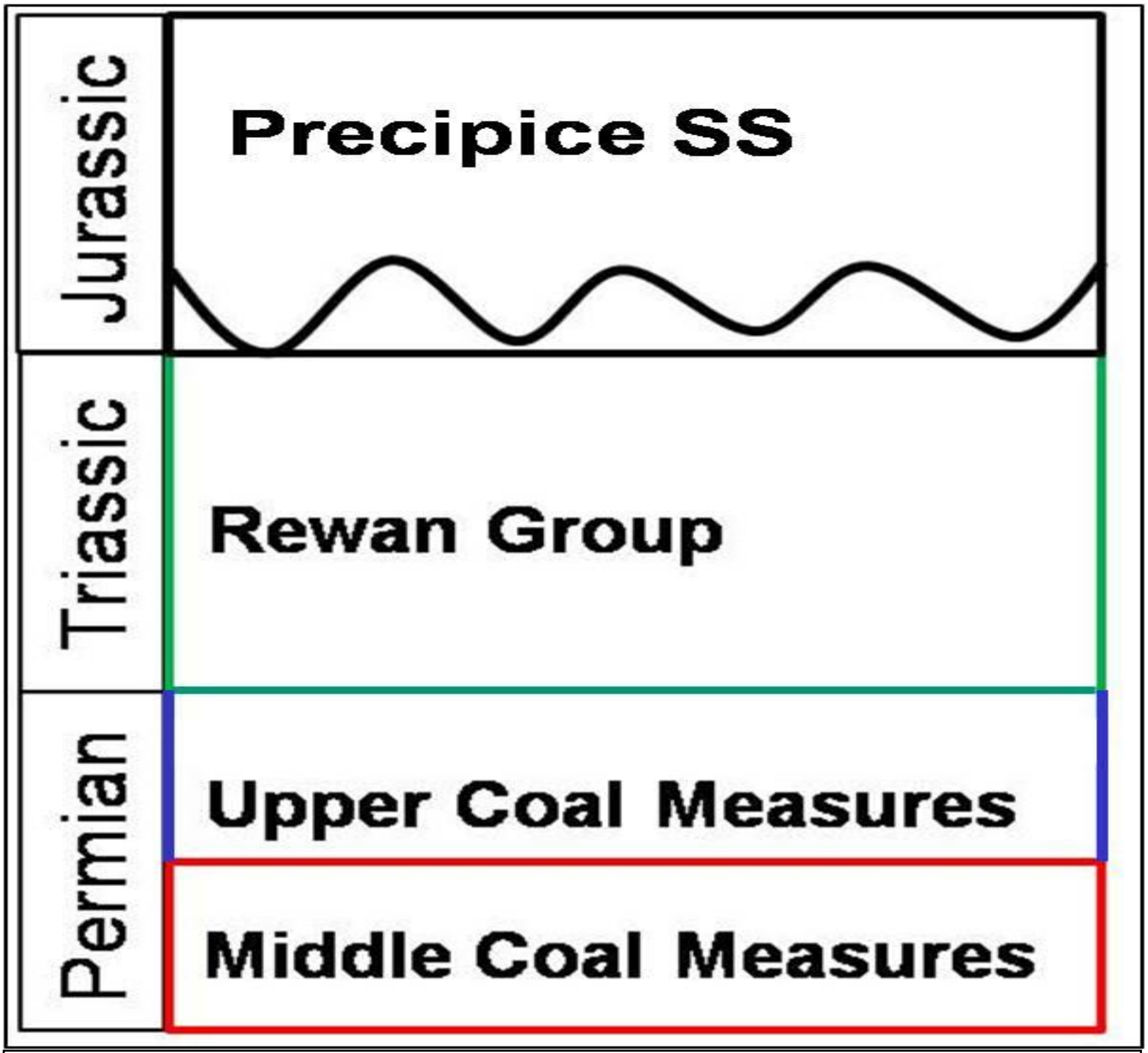

Figure 2. Stratigraphic column for the formations of interest in this study. The upper coal measures are the primary hydrocarbon bearing coal seams in the reservoir.

siltstone and claystone that lies atop the reservoir, representing an oxidized floodplain with fluvial episodes as the depositional environment. Figure 3 shows the prominent unconformity visible in the seismic data that overlies this sequence and separates the Triassic and Jurassic time periods. Figure 4 is the top coal seam horizon through the variance cube plotted with production.

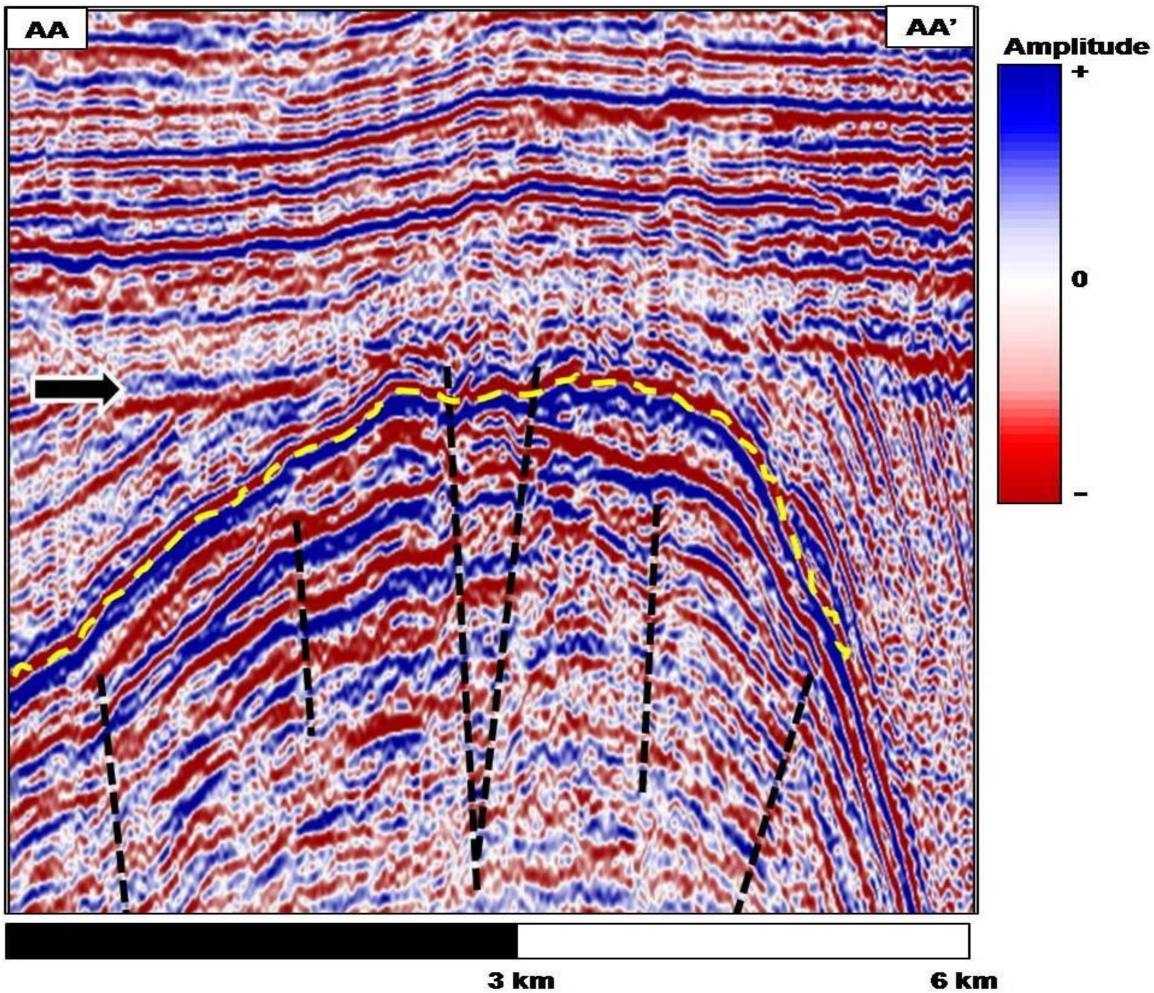

Figure 3. The coalbed-methane reservoir lies within this prominent anticline. The yellow dotted line is the top coal seam (a strong negative amplitude). The black block arrow points to the visible unconformity that separates the Triassic and Jurassic time periods. The black dashed lines are interpreted faults that have formed as a result of the folding in this area.

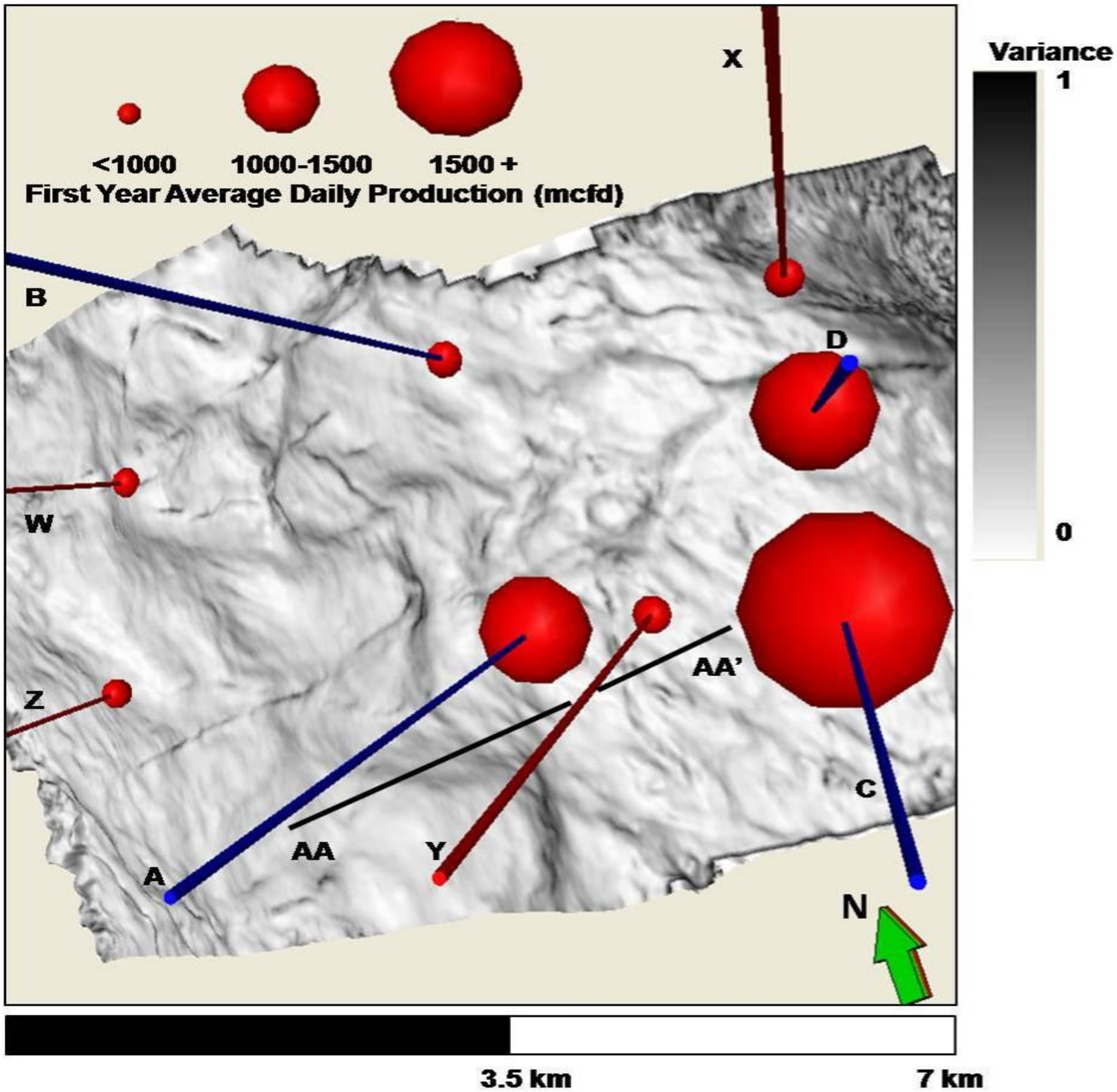

Figure 4. The top coal seam horizon through the variance cube depicting the wells in the study area. The AA – AA' line is the vertical section in Figure 3. The first year average daily production for the wells in thousand cubic feet per day are depicted by bubbles. The name of each well is listed to the left of the wellbore.

Structurally, this reservoir lies within a large anticlinal structure that Korsch (2004) has labeled an incipient fault-propagation fold. This structure resulted from a westward propagating thrust system associated with terrane accretion to the New England orogen (Figure 1). Figure 5 depicts a 2D seismic line of this structure with Korsch's (2004) interpretation of the planar, deep-seated crustal fault that is an intricate part of this fault-propagation fold formation.

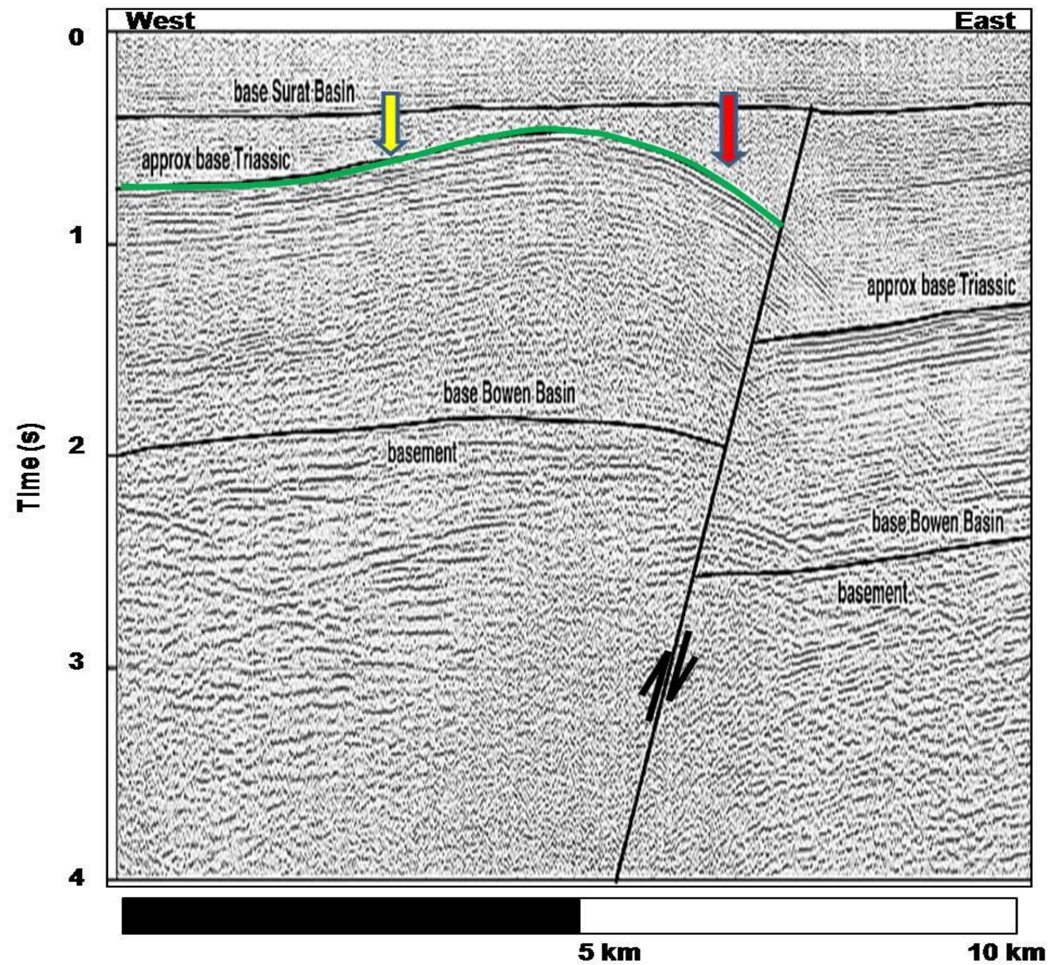

Figure 5. This 2D seismic line of the reservoir shows the top coal seam interpreted in green. The red block arrow points to the steeper front limb of the fold while the yellow block arrow points toward the more gradually dipping back limb (modified after Korsch, 2004).

The steeper front limb is to the east and the gradually sloped back limb is to the west. Imbrication or overlap of thrust slices (Suppe, 1985) can cause faults with dips greater than 20˚, especially in the forelimb and anticlinal crest. Figure 6b depicts a modeled fault propagation fold that exhibits imbricate development during thrust propagation in the forelimb (Mitra, 1990).

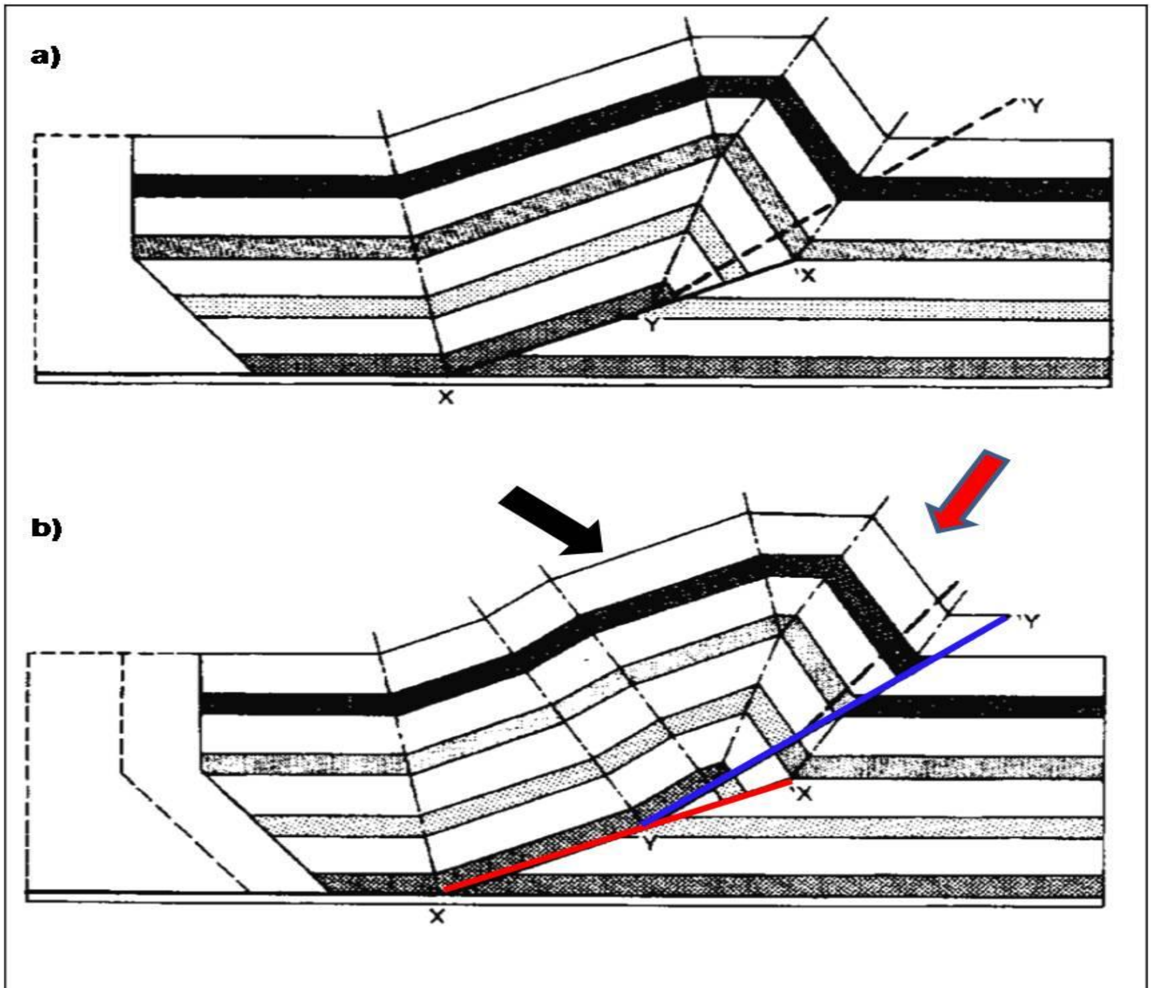

Figure 6. Diagram showing two types of modifications to a fault propagation fold: (a) progressive abandonment of deeper thrusts and (b) transfer of slip to branching imbricates. Imbricate thrusts (blue line) can form on the forelimb (red block arrow) and back limb (black block arrow) portions during thrust propagation (Bose, 2010). The master fault is designated with the red line (Modified after Mitra, 1990).

III. Coal, Cleats, and Coalbed-Methane

Coal is designated according to its rank which refers to changes that occur in the rock's organic matter with temperature, pressure and time. The Permian

Bowen Basin coals are primarily high- to medium-volatile bituminous-rank coals (Faiz, 2008). Coal is formed from compaction of plant remains in terrestrial environments such as swamps or marshes. Macerals are the plant remains in coal and make up at least 50 percent by weight of coal (AGI, 2009). Crosdale (2007) conducted a petrographic analysis of core taken from the seismic survey area that reveals the most abundant macerals in the best-developed coal seam are by average volume percent: 61% vitrinite, 34% inertinite, and 3% liptinite. The remaining 2 percent of the coal is mineral matter which is generally equated to ash content and increases the bulk density. The high vitrinite content correlates well with stratigraphic descriptions of the upper coal measures as "bright coal seams". Numerous studies (e.g., Close, 1993) note that cleats tend to be most abundant in vitreous (bright) coal lithotypes rich in the vitrinite maceral group.

In a broad sense, cleats are the linear discontinuities in coal that form a structural fabric due to physical and chemical changes during coalification (Solano-Acosta et al., 2007). Cleats can develop in coal as a result of factors such as dehydration, differential compaction, and paleotectonic stresses (Close,1993). Fractures can also be present in coal, but fractures are irregular discontinuities (on any scale) that are randomly distributed and do not follow a well-defined pattern (Solano-Acosta et al., 2007). Two main sets of cleats that form in coal beds are face cleat and butt cleat. Face cleat is typically the primary cleat set, is the tallest and longest cleat in the coal bed, and is the first fracture to form in the coal (Grout,1991). Butt cleat is the secondary cleat system that is orthogonal to the face cleat and perpendicular to bedding (Solano-Acosta et al., 2007). Figure 7 depicts a typical array of cleats within a coal bed.

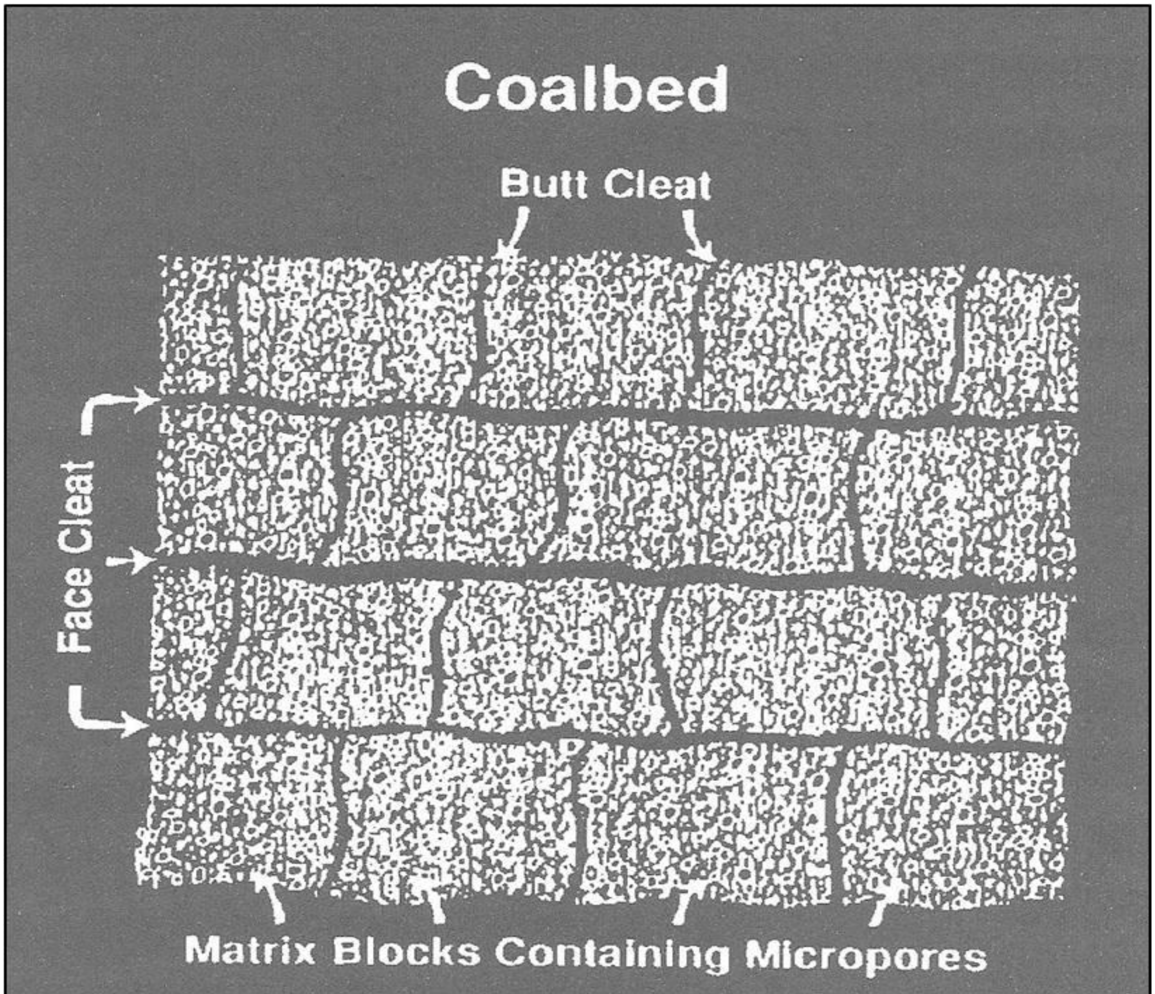

Figure 7. The face cleats are the primary fractures in coal beds and tend to be the longest and tallest fractures. The butt cleats are perpendicular or near-perpendicular to the face cleats (Close,1993) and generally have a greater cleat spacing than face cleats (After Boyer, 1989).

Cleats provide the main permeability pathway in coals for Darcy flow of gas and water. A number of factors can influence the permeability of cleats including cleat frequency, cleat spacing, cleat aperture width, and cleat mineralization. The vitrain lithotype of bituminous-rank coals, such as the ones in this reservoir, are known to behave in a brittle fashion. Due to the low matrix permeability in coal, the existence of natural fractures and cleats greatly enhances coalbed-methane production (Ramos and Davis, 1997). With a better understanding of the nature of the cleats and fractures, a company in the coalbed-methane business can harness the most of their reservoir's deliverability. The key elements of cleat analysis for coalbed-methane production are cleat mineralization, a firm understanding of the local stress regime, and determination of face and butt cleat orientation.

Coalbed-methane reservoirs act primarily as self-sourcing reservoirs, but these reservoirs sometimes also contain migrated gas from other sources (Ayers, 2002). Coalbed-methane reservoirs are dual porosity systems that derive their porosity from the micropores of the coal matrix and from cleats and fractures (Jahediesfanjani and Civan, 2005). These reservoirs are attractive because of the large surface areas of the micropore walls, capable of adsorbing more gas molecules than primary pores in conventional sandstones. To cause desorption of gas from the micropore walls and produce these reservoirs, reservoir pressure must be dropped below the saturation point. Following desorption, gases diffuse through the matrix to the cleats or fractures where they can flow to the wellbore by Darcy flow (Ayers, 2002). Figure 8 illustrates the gas transport mechanisms of coalbed-methane production beginning with adsorbed gas. Coalbed-methane wells often have a dewatering stage that occurs with initial production, where it is not uncommon for water production to decline and gas production to increase with time (Ayers, 2002).

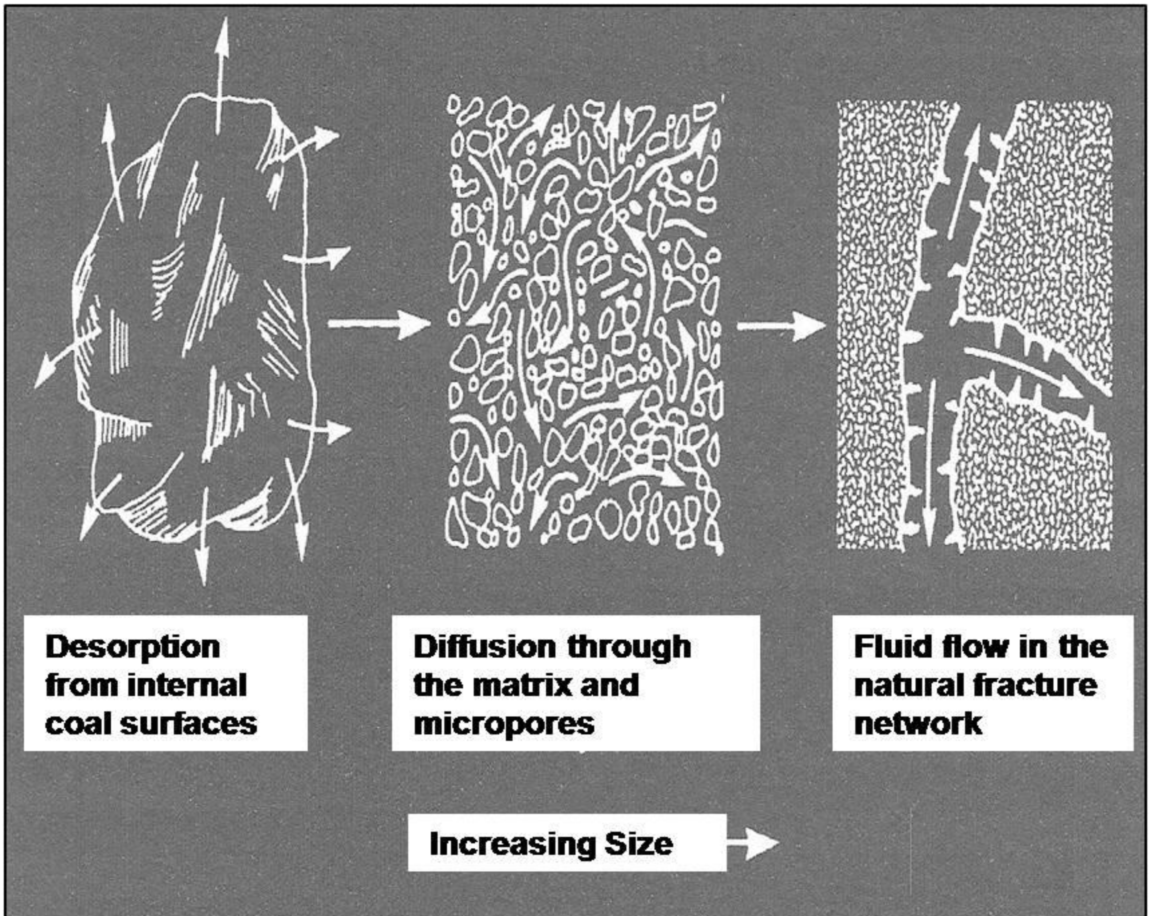

Figure 8. The production of adsorbed coalbed-methane starts with desorption of gas from the micropores. Next, the gas diffuses through the matrix to reach cleats or fractures, after which the gas will flow to the wellbore. (Modified after Boyer, 1989).

Figure 9 displays schematic diagrams of decline curves for two different types of coalbed-methane wells. Coalbed-methane wells can display negative decline as they go through the dewatering stage (Figure 9a) or the wells may display a relatively gradual decline in lower permeability areas (Figure 9b). Furthermore, bituminous-rank coals are considered to be more prolific in the generation of thermogenic methane (Figure 10). Figure 11 depicts where this peak generation window falls when considering the range of coal bulk density values and ash contents of Kaiser et al.'s (1995) model.

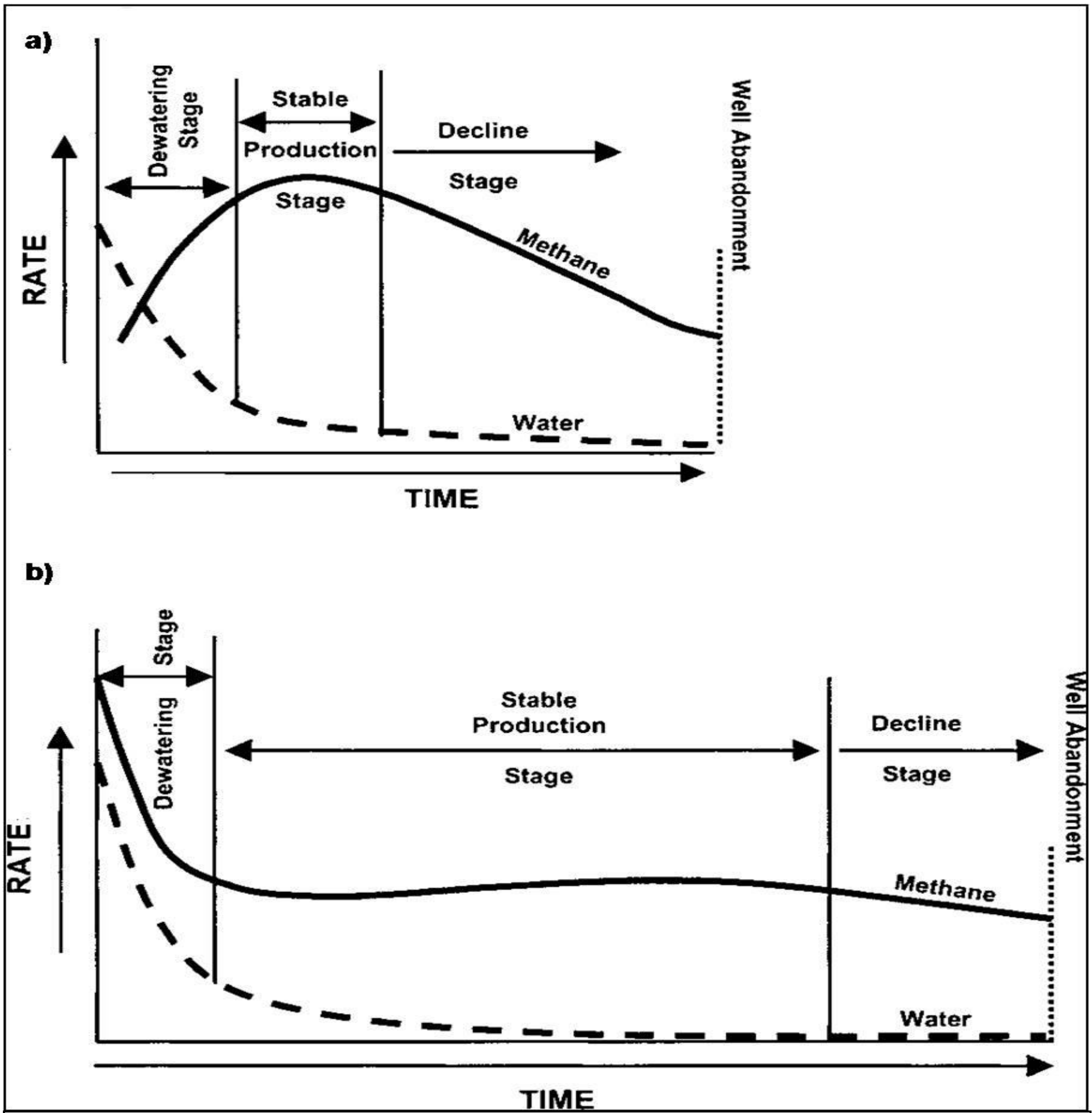

Figure 9. (a) A coalbed-methane decline curve shows the inverse relationship that some of these wells have between water and gas production during the dewatering stage. (b) A decline curve indicative of a lower permeability coalbed-methane well. (Modified by Ayers, 2002; from Schraufnagel, 1993).

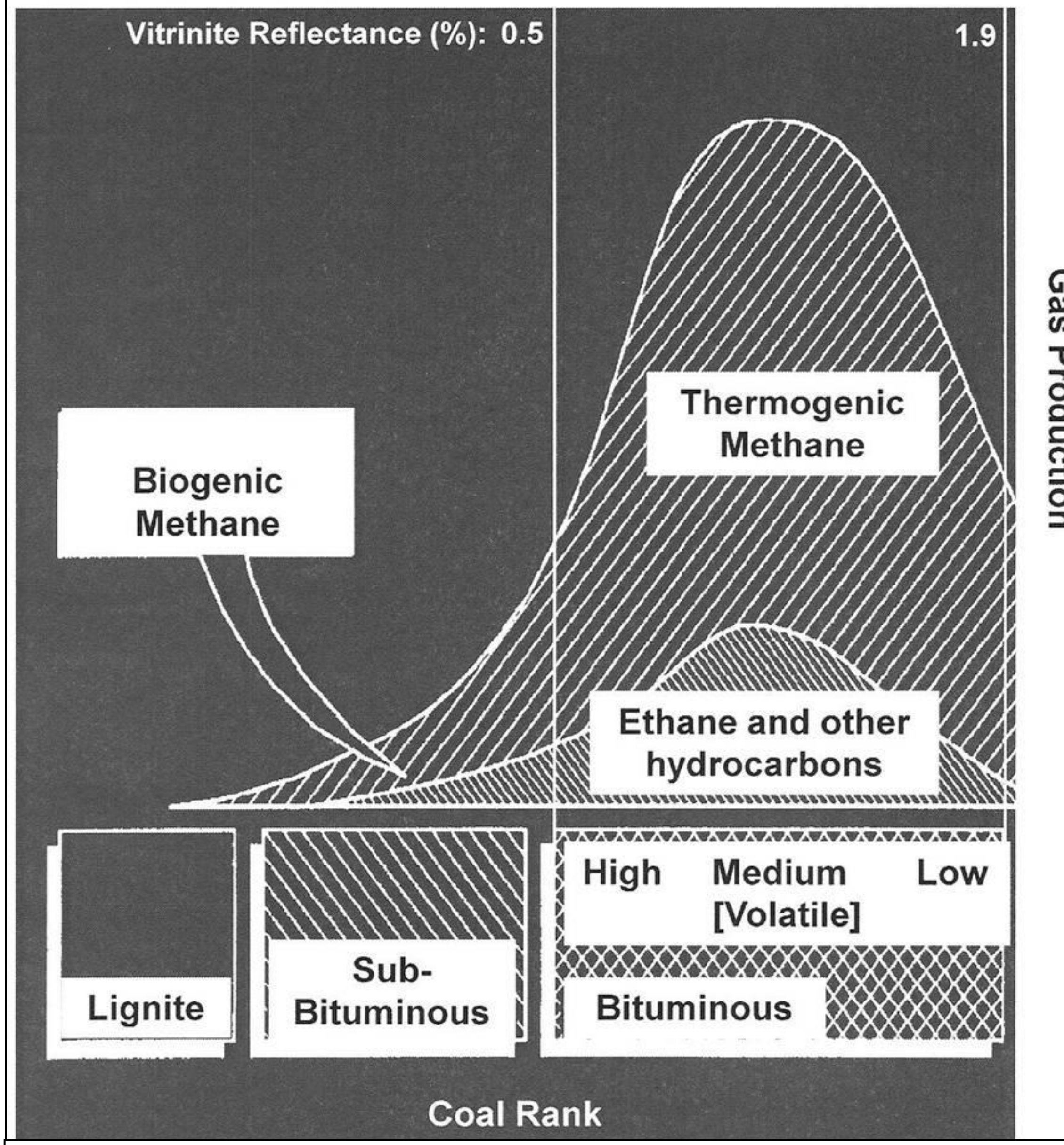

Figure 10. The peak window for thermogenic methane generation in coal corresponds to bituminous-rank coals as seen in the above diagram with the respective vitrinite reflectance values that correspond with the lower and upper limits of bituminous-rank coals according to Taylor et al. (1998) (Modified after Boyer, 1989).

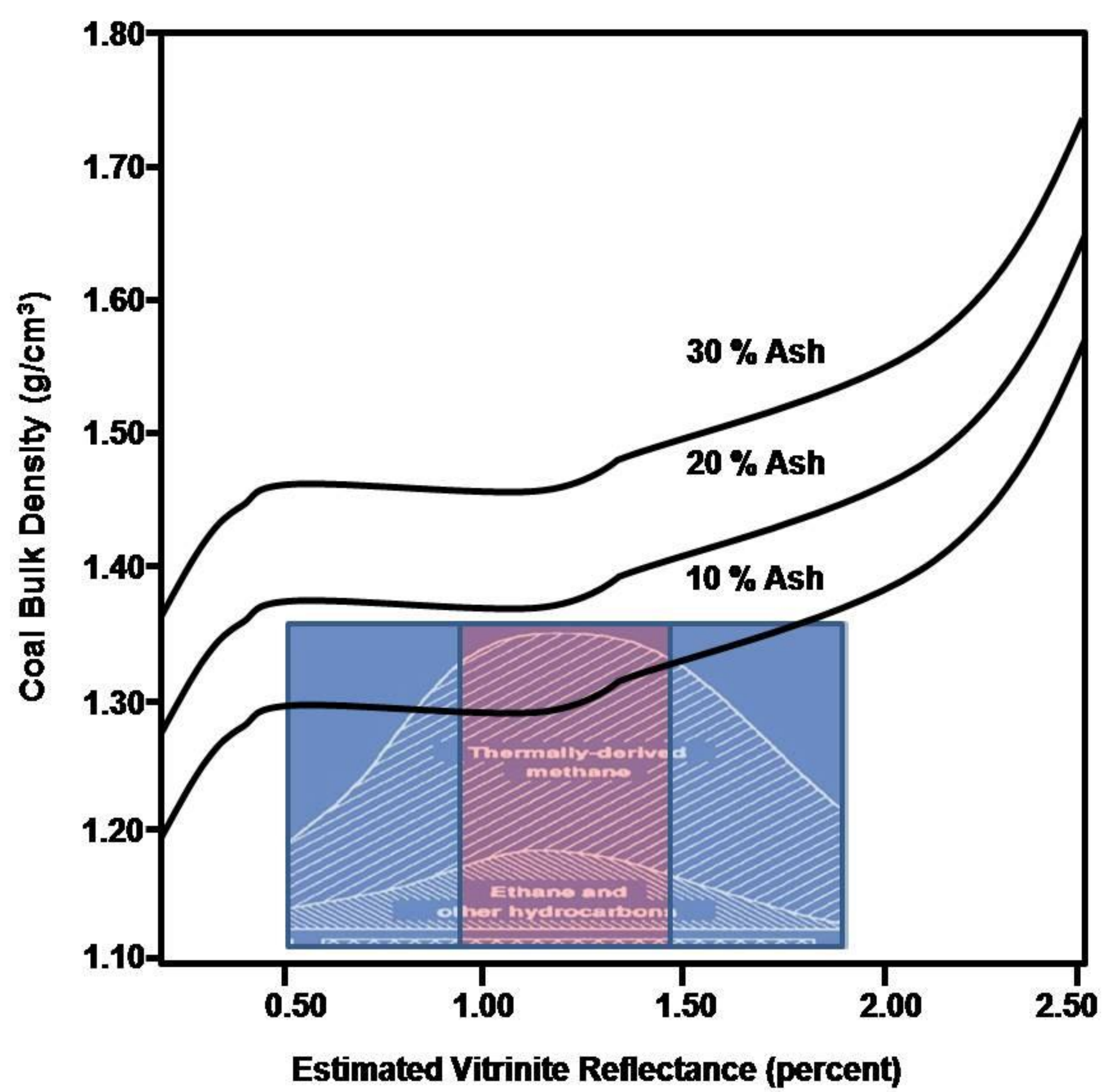

Figure 11. Bulk coal densities as they relate to ash content, vitrinite reflectance, and peak methane generation. This chart makes it evident that for similar vitrinite reflectance values, coals with higher bulk densities have higher ash contents. Additionally, coals with similar ash contents and vitrinite reflectance values above 0.5 % have optimal levels of gas generation (Modified after Kaiser et al., 1995).

Cleat aperture widths have significant control over the flow of fluid through coal seams as it appears in the equation for fracture permeability, k_f,

$$k_f = \left(\frac{w^3}{12Z}\right), \tag{1}$$

where *w* is the cleat aperture width and *Z* is the average cleat spacing in coal (Nelson, 2001, Figure 12).

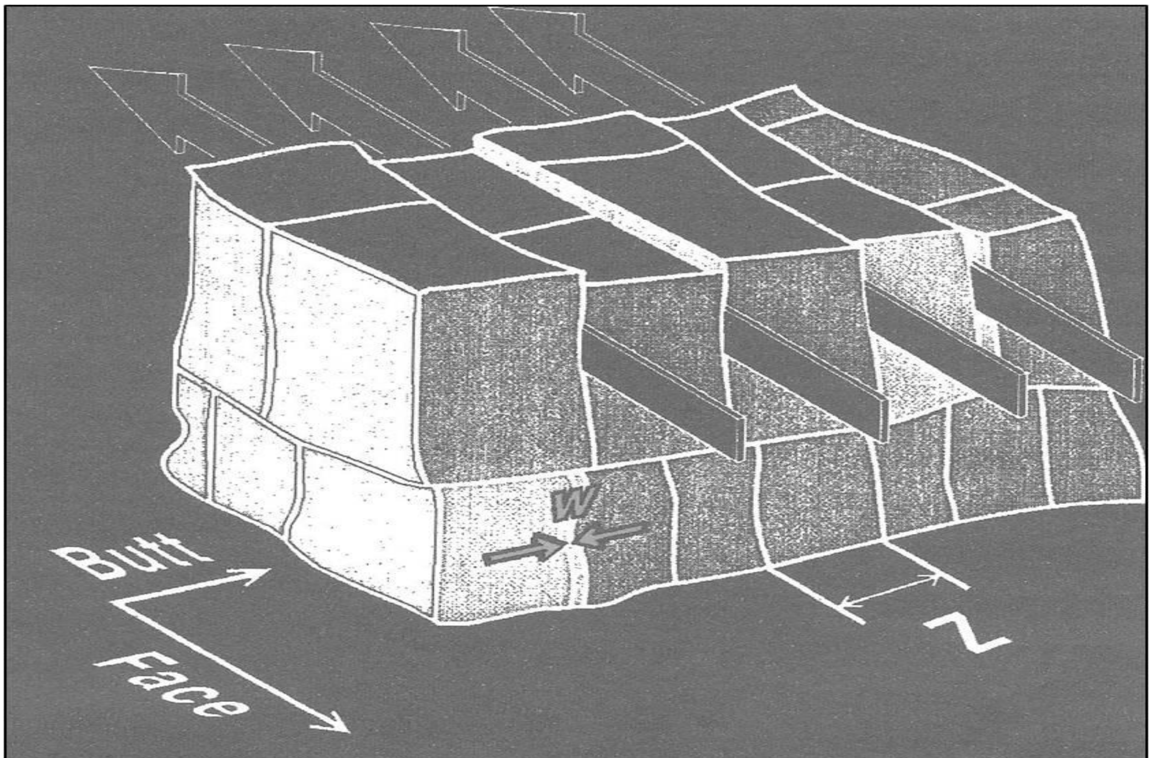

Figure 12. Depiction of a coal block showing the variables that influence the fracture permeability (Nelson, 2001) in coal defined by the equation $k_F = w^3/(12*z)$, where k_F is the fracture permeability, *w* is the cleat aperture width, and *z* is the average cleat spacing (Modified after Scott, 2000).

Diagenetic alteration is an important element of cleat development to consider. Mineral-fill of the cleat apertures through diagenetic processes reduces permeability. Close (1993) notes that the most common minerals filling cleat apertures of bituminous coals are carbonates and sulfides. Calcite is possibly the most common culprit of cleat mineral-filling. Additional mineral matter in coals can consume space otherwise occupied by organic matter, or minerals can fill fractures and cleats and stifle fluid flow. Image logs can be an effective tool at the identification of mineral-filling and flow barriers. The heightened vertical resolution is a distinct advantage of this tool. The operator has discovered that these logs reveal small scale mineral heterogeneities that can impede cleat and fracture permeability within coal seams.

IV. Seismic Data Quality

The data consist of a 3D seismic survey in Queensland, Australia, numerous 2D seismic lines, and azimuthal gathers for the 3D survey. The operator's primary goal for this survey was the improved mapping of the upper coal horizons within the basin. Geco-Prakla acquired the seismic data in October and November 2000. The data were recorded using 45 source lines with a 200 m interval and 23 receiver lines with a 200 m interval (Figure 13), resulting in a natural bin spacing of 25 m x 12.5 m.

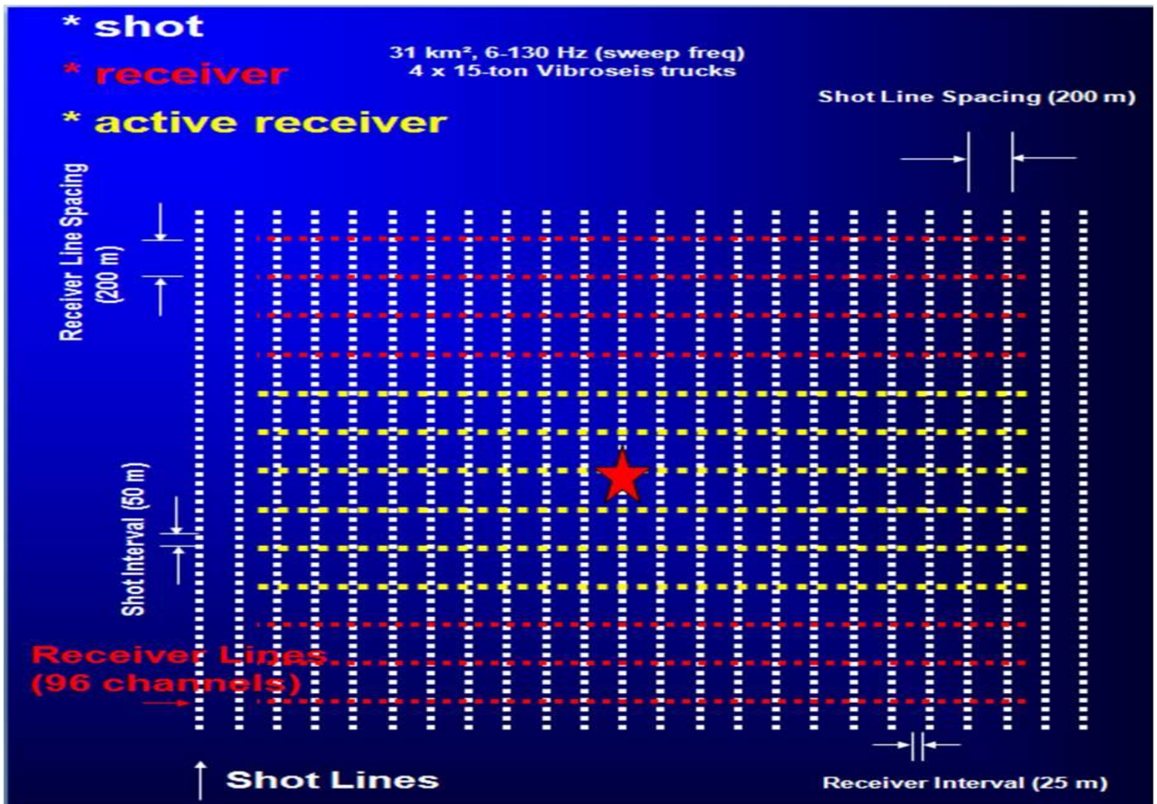

Figure 13. The geometry for the 3D survey in the Queensland area . Shots were at the center of 96 channels spaced 25 m apart, accounting for maximum offsets of 1,200 m.

The survey size is 31.56 km^2 of rolling farmlands in Queensland, Australia. The acquisition company used four Mertz M26 vibrators vibrating with a sweep length of four seconds and a sweep frequency range from 6-130 Hz. Group arrays consisted of twelve sensor SM4, 10 Hz geophones in a linear array with the source in the middle of each line, resulting in a multiplicity of 36 fold. The sampling rate of the data is 2 ms. Pre-stack processing parameters included surface consistent deconvolution, 10-110 Hz spectral whitening, and spatial dealiasing dip moveout (DMO). Some of the final post-stack parameters were spectral balancing between 10-110 Hz, *f-x* deconvolution, and modified residual migration with 100% smoothed velocities. Figure 14 shows the final spectra for the target interval encompassing the upper coal measures.

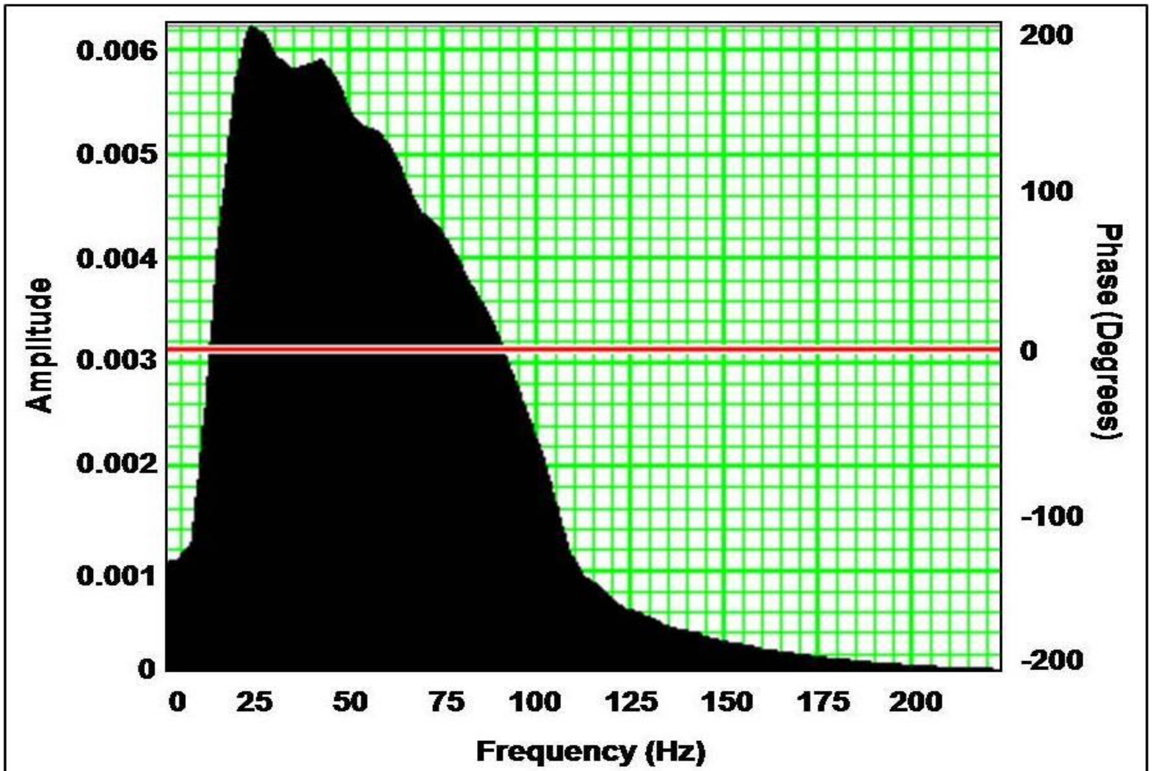

Figure 14. The final amplitude spectrum of the target interval (Upper Coal Measures). The bulk of the data lies within the frequency range of 10-110 Hz.

The operator drilled all of the coalbed-methane wells in this study following the seismic survey. The operator provided a suite of well logs for 10 wells within the 3D seismic survey area. Five of the wells have gamma ray, P-wave sonic (DT) and density (RHOB) logs that are most useful in the well ties process. Figure 15 is a view of the well logs juxtaposed with the seismic during the well ties process.

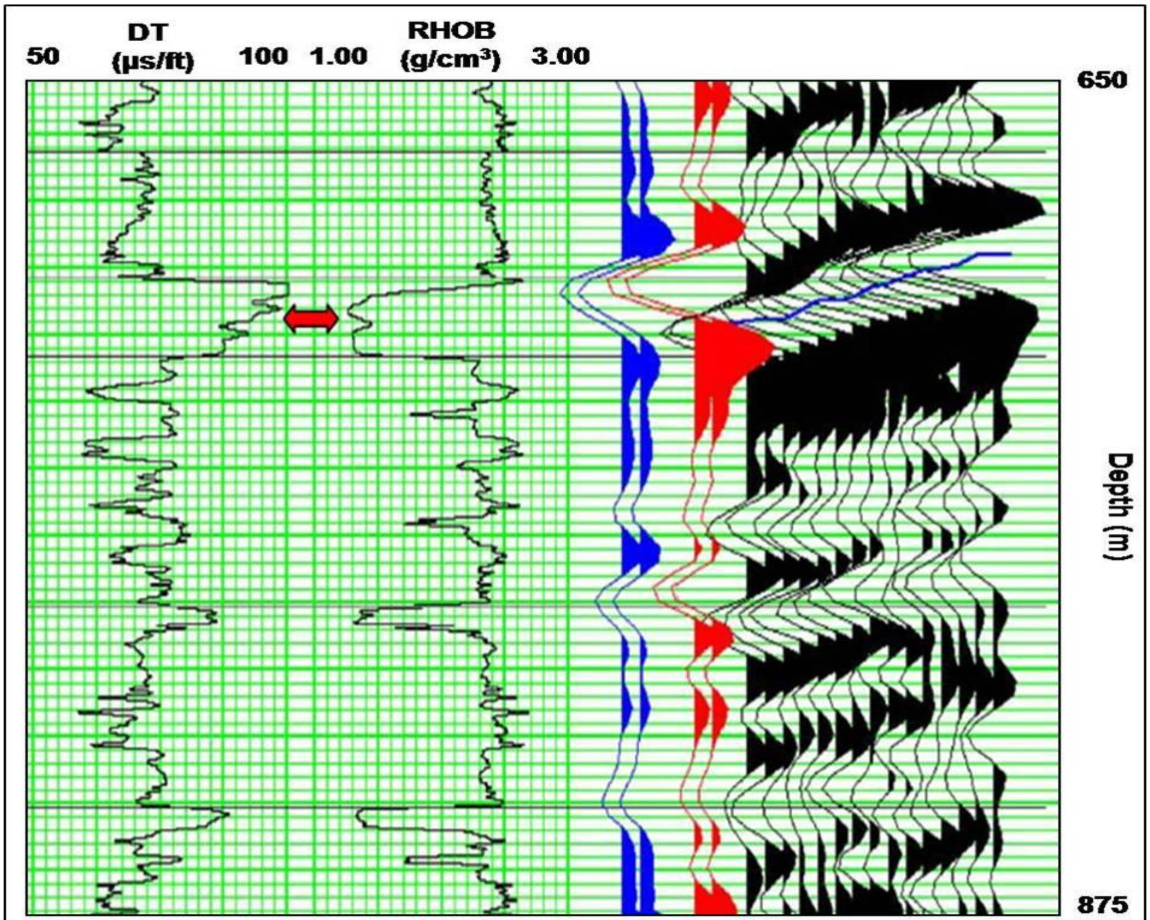

Figure 15. From left to right, the panel shows the P-wave sonic log, the density log, the synthetic traces, the composite traces, and the seismic data. The red double block arrow points to the top and most developed coal seam in the reservoir. Note the composite traces represent the trace at the center of the seismic display.

The production data for the field consist of daily gas and water production for eight of the wells. The operator provided checkshots and synthetic-generated TD curves for nine wells. Additionally, the operator interpreted a seismic horizon for the top of the C2 coal seam which they provided to facilitate the interpretation process.

The operator also supplied a University of Queensland report of core analysis that was conducted on coal core samples from one of the wells in the survey area. The core report presents the results of numerous stress-strain tests conducted under various conditions. These results include calculated values for Young's modulus and Poisson's ratio determined from the measured values of stress and strain. A petrographic analysis of core from the same well presents a detailed breakdown of the maceral and mineral compositions. Finally, a core desorption report produced by an affiliate of the University of Queensland reveals information on the core gas content and the gas content relationship to temperature, diffusion rates, and coal stress relief due to desorption for the same well used in the stress-strain report.

V. Seismic Estimation of Deliverability in Coal

For the purposes of this study, I define *deliverability* to be those conditions that exist in the reservoir or those coal characteristics that are well-aligned with optimal gas production rates in this gas field. Locations of good deliverability might also be called "sweet spots". Mapping deliverability is key to optimal well placement and the primary objective of 3D seismic amplitude and attribute analysis.

I begin by considering a gas-in-place equation for coalbed-methane reservoirs in which Mavor and Nelson (1997) define *GIP*, the gas-in-place (scf), by

$$GIP = 1{,}359.7 h A \rho GC, \tag{2}$$

where *h* is defined as the coal thickness (ft), *A* is the drainage area (acres), *ρ* is the ash-free coal density (g/cm^3) defined as the lowest value on the density log, and *GC* is the ash-free gas content (scf/ton). In this study, I will only attempt to directly resolve the density variable. I will attempt to indirectly resolve variables of drainage area and gas content through consideration of structure and permeability.

The seismic attribute peak frequency can provide indications of coal thickness, *h*. Thin bed reflections have a characteristic frequency domain expression that indicates temporal thickness in seismic data (Partyka et al., 1999). The peak frequency together with peak amplitude, trough frequency and trough amplitude can effectively characterize the spectrum of thin coal seams (Marfurt and Kirlin, 2001). Further resolution of thickness and lateral impedance changes can be derived from the individual spectral magnitude components.

Because acoustic impedance is the product of density and velocity, impedance inversions can provide useful information regarding the coal's density (and mineral content) throughout the reservoir. Areas of low impedance can often be connected to relative decreases in coal density. The spectral magnitude components are also related to coal density. The dominant (or tuning) frequency is inversely proportional to the coal velocity and thickness. Furthermore, the coal velocity response is statistically correlated to density of the coal.

The drainage area, *A*, is related to the permeability in the sense that coal sections with higher permeability have more cleat connectivity within the coal seam allowing increased areal access to hydrocarbons. Numerous coal studies note enhanced production correlates with fracture and cleat intensity. Seismically, curvatures computed at given azimuths can reveal fracture swarms, systematic fracture sets, and cleat directions that allow for increased clarity in wellbore trajectory planning. Because the flow of methane and water will be enhanced when drilling a horizontal lateral in a direction perpendicular to face cleats, curvatures are a useful seismic tool in determining the face cleat directions and accessing greater drainage area. Amplitude versus azimuth analysis computed on acoustic impedances can also provide insight to the face cleat directions which should parallel the highest acoustic impedance and fast compressional wave direction.

Finally, the gas content, *GC*, can be related in some regions of coalbed-methane reservoirs by time structure and dip magnitude. Although migration of hydrocarbons is not suspected to be prevalent in coalbed-methane reservoirs due to the low matrix permeability in coals, seismic time structure and dip magnitude maps can provide some insight into the location of gas accumulations as a result of gas migration updip and into structural traps. Furthermore, time structure maps may also reveal areas where the coals may have undergone too much or too little thermal maturation and missed the conditions for optimal gas content. Figure 16 is the time structure map for the top coal seam. This picture shows that high producers are more prominent in the peak of the anticline. However, low producers are also present at this structural high, interspersed with the higher producers, which leads to other seismic methods of investigation into this variability.

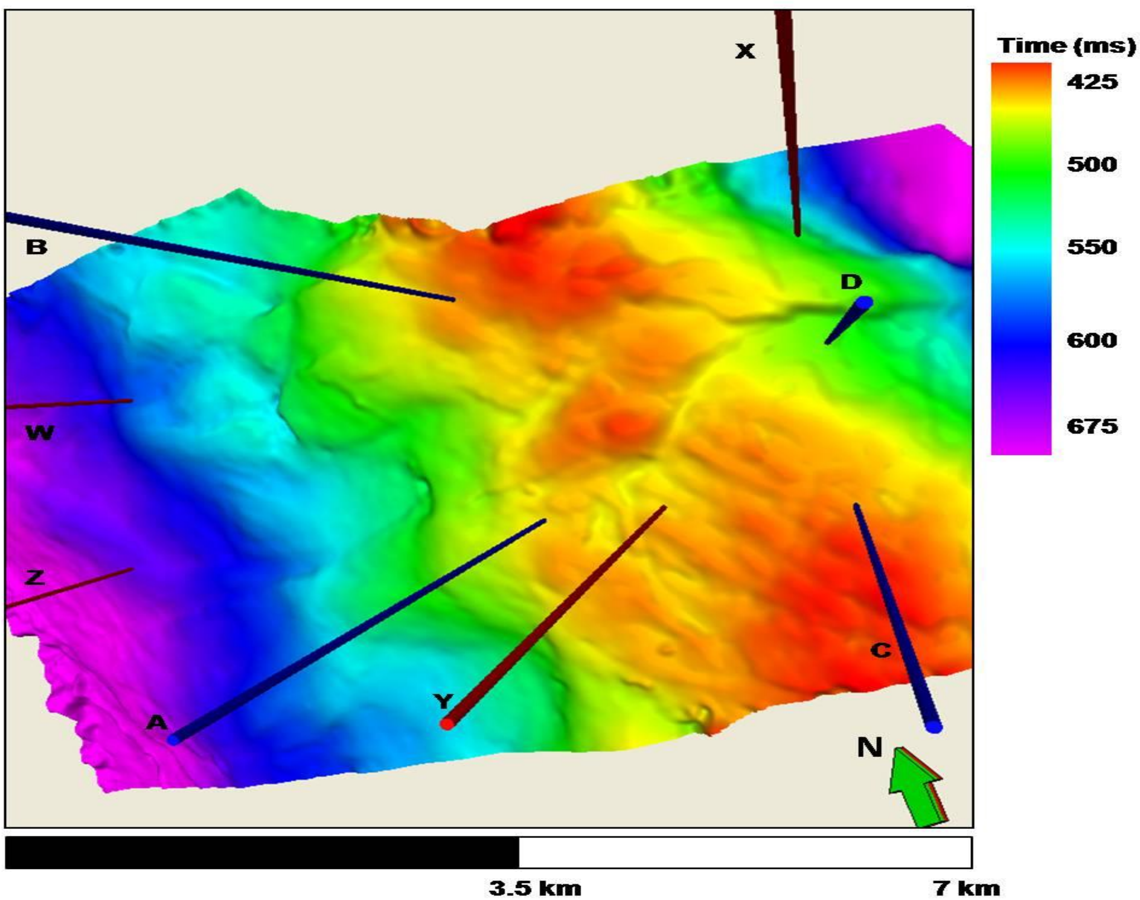

Figure 16. Time structure map of the top coal surface. Note the asymmetric geometry of the fold. The gradual western back limb does not have any high producing wells (blue wellbores). The top of the anticline has high producers intermingled with low producers (red wellbores).

VI. Multiattribute Transforms: A Link Between Seismic Data and Rock Properties

Well logs provide direct measurements of density, velocity, lithology and porosity at discrete well locations. Densely acquired seismic data provides an excellent image of structural and stratigraphic complexity, but only less direct estimates of rock properties.

Multiattribute transforms are one way in which we can integrate the rock property information from well logs with the seismic data. Once the wells have been tied to the seismic data, the interpreter generates a number of sample and/or horizon-based seismic attributes. Then, a nonlinear or linear multiattribute transform is derived between the well logs and some combination of the seismic attributes (Hampson et al., 2001). In the linear application, Hampson et al. (2001) show that we can predict a well log rock property value such as density, $\rho(t)$, away from the well at a time sample t, by

$$\rho(t) = w_0 + w_1 A_1(t) + w_2 A_2(t) + w_3 A_3(t), \qquad (3)$$

where A_i are the attribute values at the prediction location, and w_i are unknown weights. The weights can be estimated by the minimization of the mean-squared prediction error, E^2, between the predicted $\rho(t)$ and the real density log, ρ_i, given by the equation:

$$E^2 = \frac{1}{N}\sum_{i=1}^{N}(\rho_i - w_0 - w_1 A_{1i} - w_2 A_{2i} - w_3 A_{3i})^2, \quad (4)$$

where N is the number of data points in the well log being predicted by the transform. Thus, the result of equation 4 represents a goodness-of-fit measure for the transform where the x-coordinate is the predicted log value crossplotted with the original log value as the y-coordinate. The weights in this equation can be obtained through the normal equations. The best attributes are selected through a procedure known as stepwise regression (Draper and Smith, 1966). In stepwise regression, the weights and training errors are calculated for each seismic attribute, one at a time. The attribute with the lowest error becomes the A_1 term in equation 3. Then, the procedure is repeated using A_1 to find the second attribute that gives the lowest error for the combination of A_1 and A_2. This process is repeated until we reach a user-defined optimum number of attributes. The diagram in Figure 17 summarizes this multiattribute transform process.

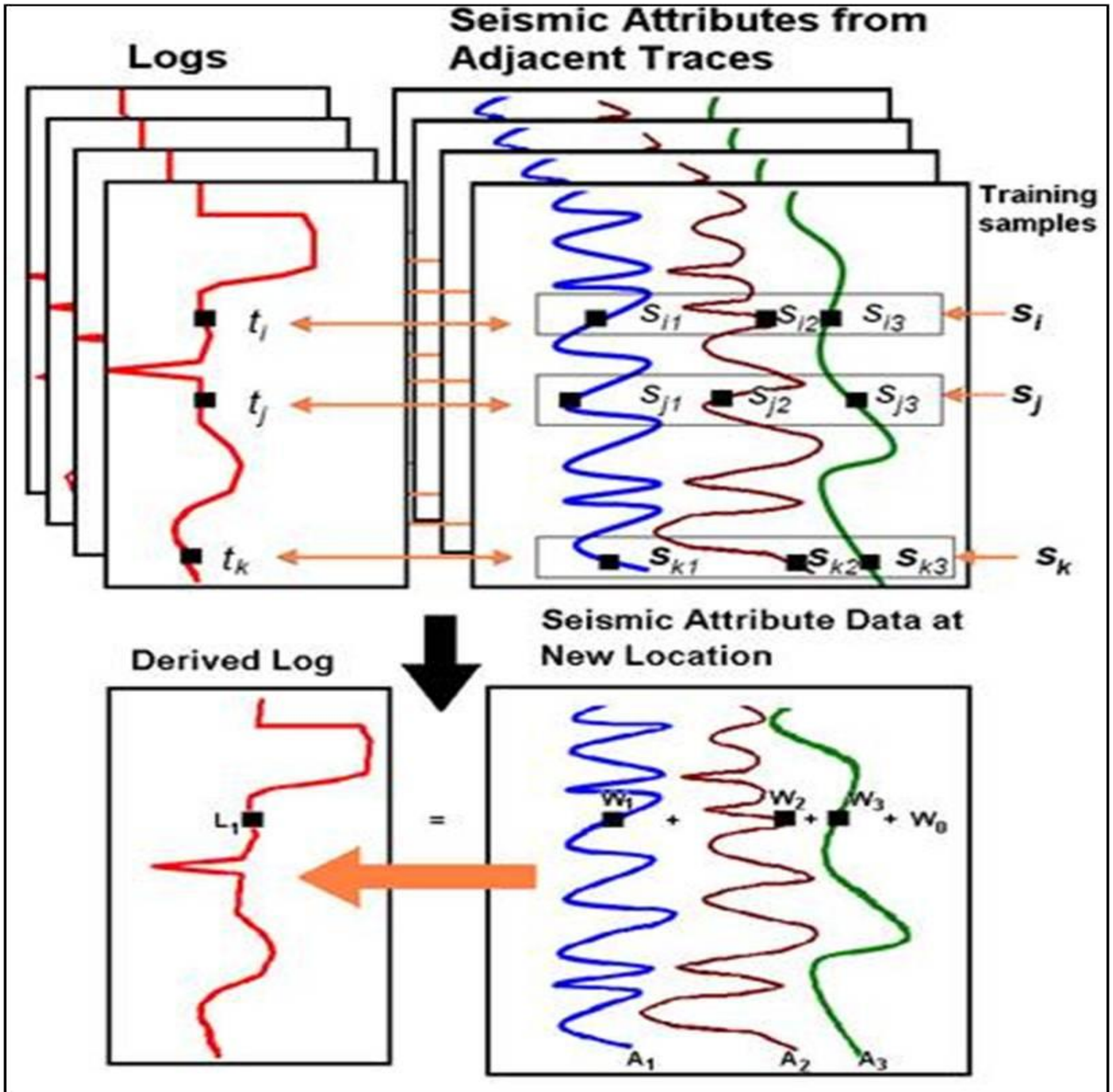

Figure 17. The multiattribute transform process, where seismic attribute data samples at a well location are correlated with well log data points to derive a mathematical relationship that can be used to predict well log properties away from well locations within a seismic data survey. L_i is the predicted log value at the *i*th time sample, t_i is the original log value at a given time sample, S_{in} is the *n*th attribute's value at the *i*th time sample, and w_i is the weight of the respective attribute at the *i*th time sample (after CGG Veritas, 2007).

Initially, the process requires the application of equation 4. The resultant error is referred to as the training error and represents the error when all input wells are considered. The validation error is determined by hiding one of the wells in the training step and predicting its value after training on the remaining wells. The final validation error represents the average of the single well validation errors resulting from repeating the process as many times as the number of wells (Pramanik et al., 2004).

A. Multiattribute Transform and Rock Properties Case Study

Boyer (1989) showed that the coal ranks that correspond with peak production of thermogenic methane are high-, medium-, and low-volatile bituminous-rank coals (Figure 10). Additionally, Taylor et al. (1998) correlated vitrinite reflectance values from 0.5-1.5% to high- and medium-volatile bituminous-rank coals. Finally, Kaiser et al. (1995) shows that low bulk densities in coal corresponded to vitrinite reflectance values and ash contents consistent with the coal ranks and ash contents in this survey and consistent with high thermogenic methane production for coals (Figure 11). The Kimmeridge and other shales have bulk densities that decrease with increasing total organic carbon (TOC) content (Rai, 2009). For vitrinite reflectance, R_o>0.5%, coal with low bulk densities and similar ash contents can be associated with higher gas content. In this study, I use the RHOB logs as the primary bulk density values. I follow Yee et al. (1993) who assume that the lowest density value in the density well log is nearly ash-free. Ash-free coal bulk density values in the top coal seam of the wells range between 1.25 - 1.34 g/cm^3.

Examining Figure 4, I note that Wells A, B,C, and D produced above average amounts of gas, exceeding 1,000 thousand cubic feet per day (mcfd) for the first year. Wells W, X, Y, and Z produced below 500 mcfd on average for the first year. Kalkomey (1997) observed a high probability of spurious correlations between well measurements and seismic attributes when the number of wells is small, as in this study. For these instances, Kalkomey (1997) recommended using only those seismic attributes that have a physical relationship with the reservoir property measured by the well log. For this reason, the only seismic attributes I considered for correlation were the spectral components and the colored and bandlimited acoustic impedance inversions. I used colored inversion instead of model-based inversion because the complexity of the coal seams in the survey results in a spatially varying estimated wavelet. Colored inversion only uses a specified wavelet to test for a residual constant phase rotation in the last step (Lancaster and Whitcombe, 2000). With seismic data, 15 seismic attributes and the density logs for the wells as input, I derived a multiattribute transform that predicts density across the seismic survey through the application of equations 3 and 4. Attributes A_1 - A_3 are colored acoustic impedance inversion, 54 Hz spectral magnitude component, and the square of the 124 Hz spectral magnitude component, respectively. Figure 18 shows horizon slices of the three attributes used in the transform and the resulting predicted density horizon slice. This multiattribute transform resulted in a training error of ± 0.23 g/cm^3 with a correlation of 0.70 between the predicted density and the actual density values.

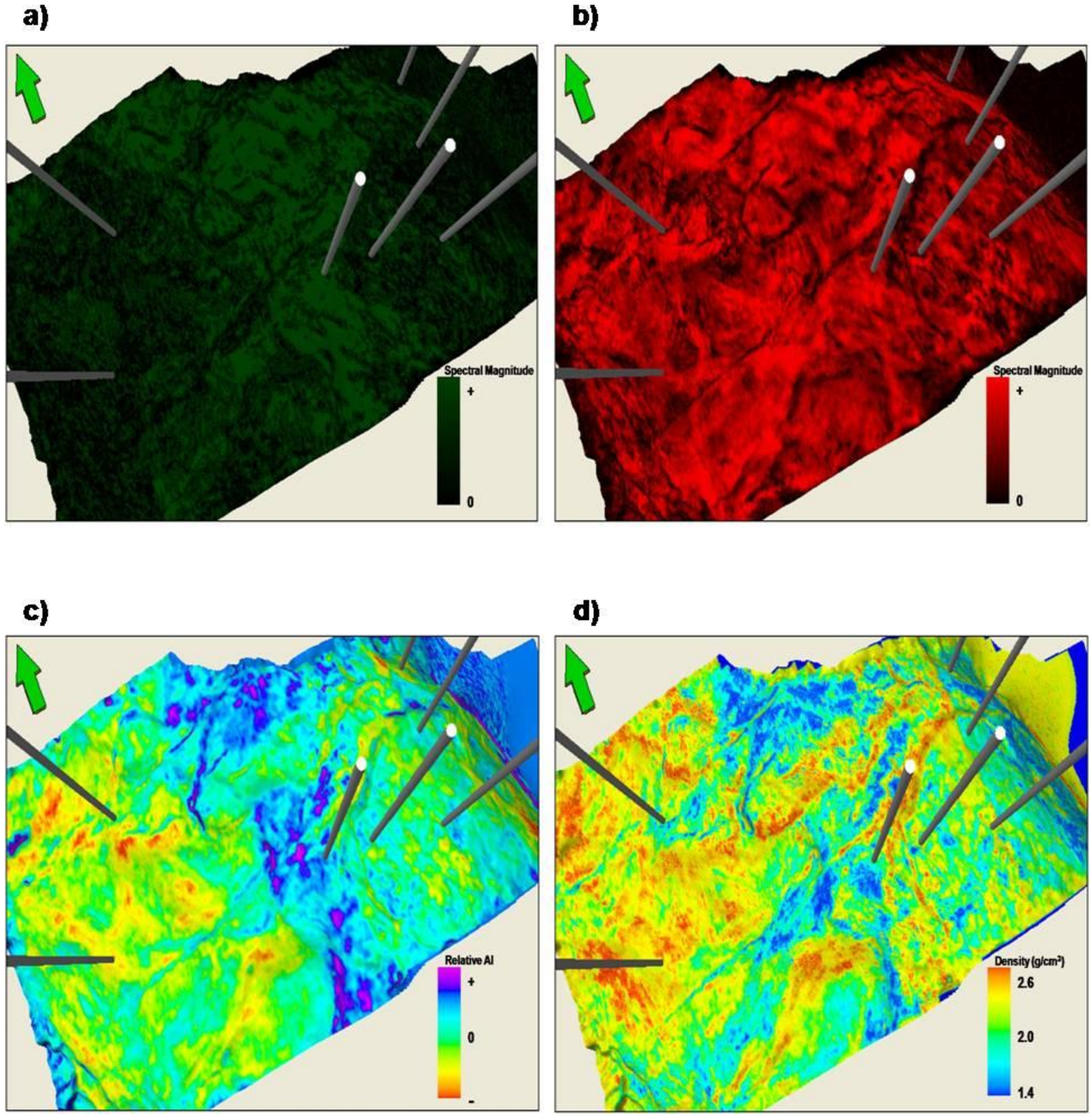

Figure 18. Horizon slices of the top coal seam showing the three attributes that are used in the transform to predict the density values: a) the 124 Hz component (squared), b) the 54 Hz component, c) the colored inversion , and d) the predicted density result.

Figure 19 shows the resulting density curves at the respective well locations. Because of the low-frequency nature of seismic attributes in comparison to well logs, the predicted density curve rarely achieves the level of spikiness exhibited in the well logs (Hampson et al., 2001). Figure 20 is the predicted density result for the interpreted top coal seam of the reservoir that forms the upper layer of the anticline.

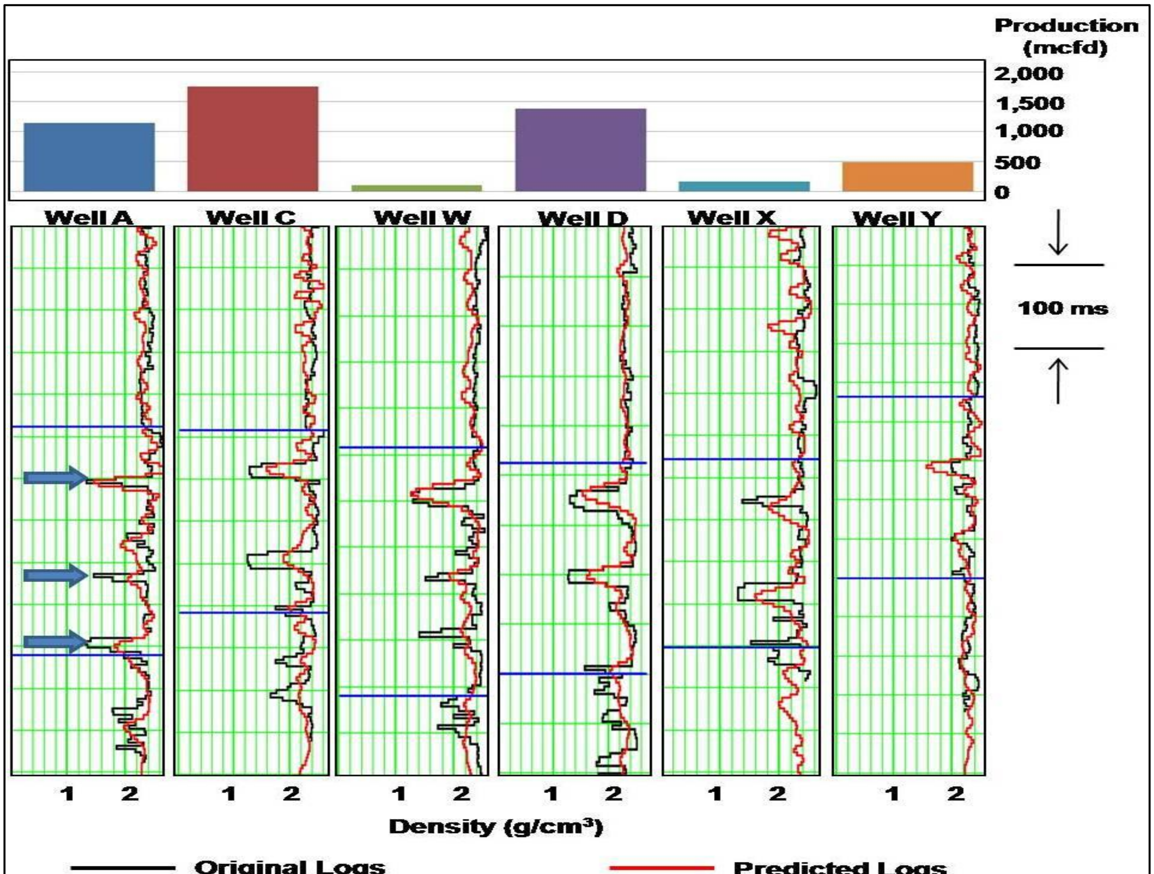

Figure 19. Panels comparing the measured density logs with the predicted values from the multiattribute transform. The analysis windows for the reservoir are annotated by the blue lines. The block arrows in the panel for well A indicate three coal seams. The correlation between the actual and predicted logs was 0.70. The first year's average daily production in thousand cubic feet per day are shown above the panels.

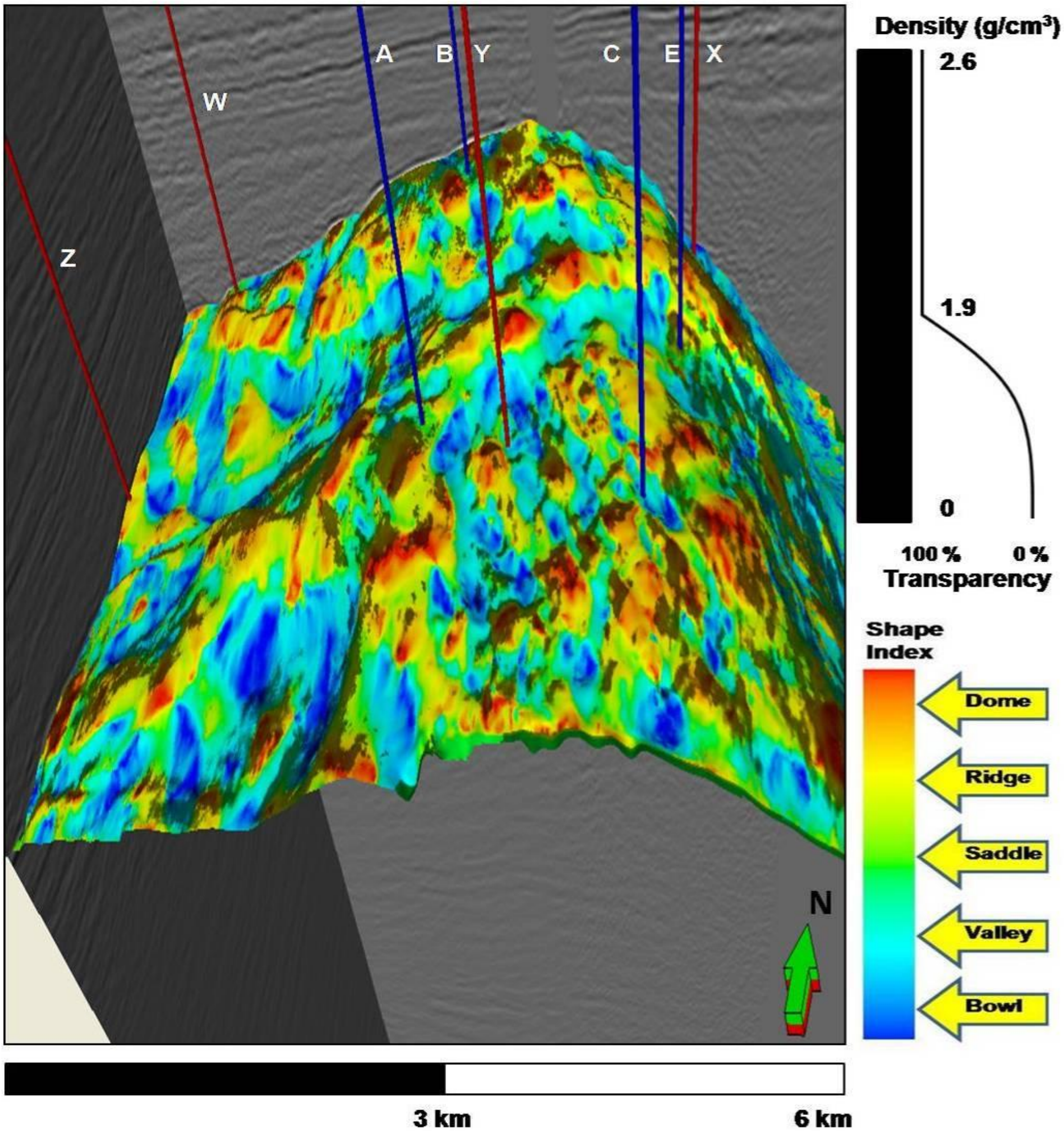

Figure 20. The top of the coal seam is displayed as predicted density values from the multiattribute transform co-rendered with the shape index volume. Density values above 1.9 g/cm^3 have been made transparent. The dark patches of low density correlate with domes and ridges remarkably well.

Using this density volume, I compare areas of lower production with higher production considering the idea that lower densities could indicate less ash content and possibly a more organic-rich coal. The results of my analysis reveal some positive correlations and also illustrate the complexities (such as cleats and fractures) of these reservoirs that cannot be explained by lithology alone. Figure 21 is a plot of the coal bulk density (from well logs) for the top coal seam versus the normalized gas production.

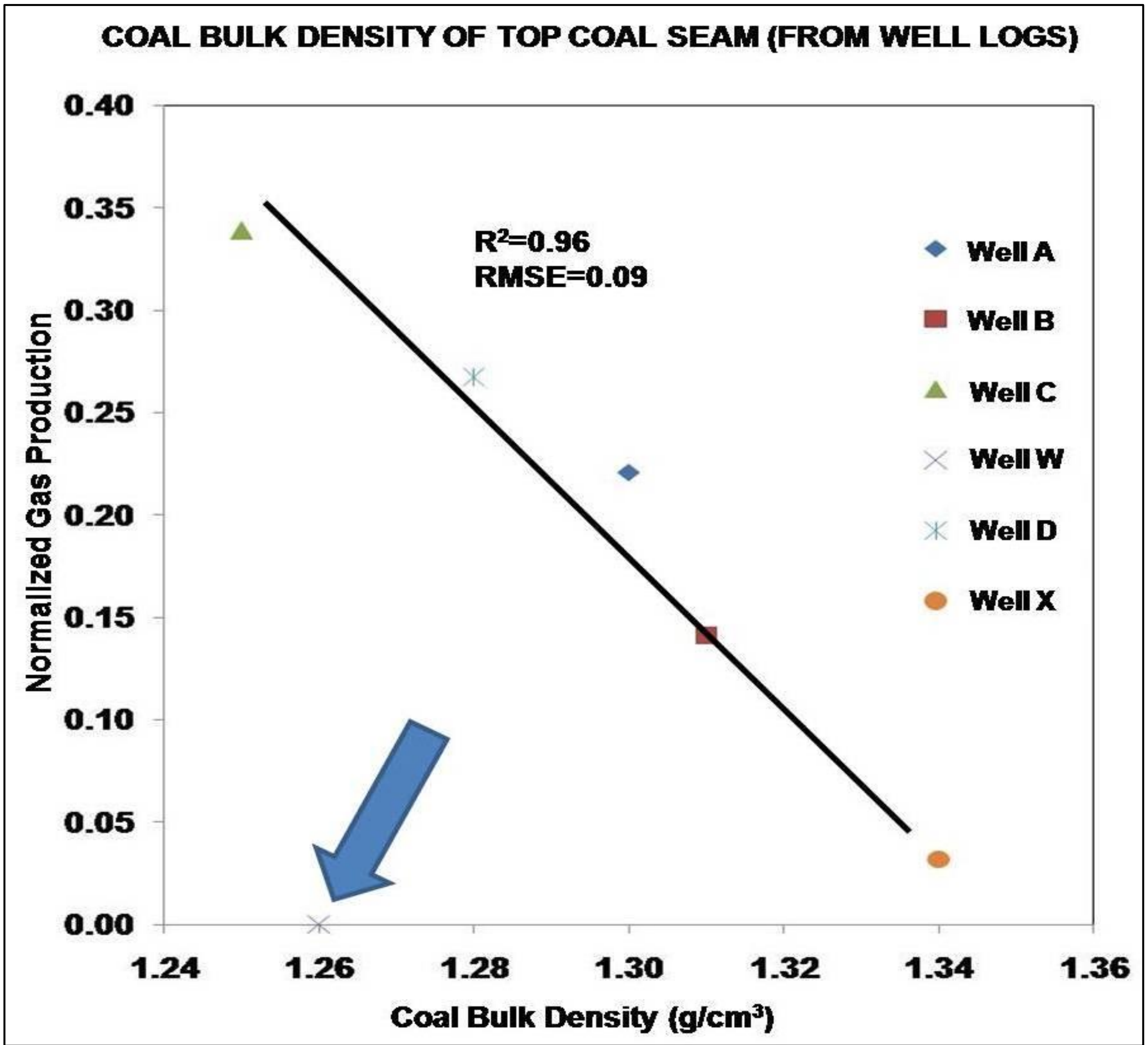

Figure 21. A plot of normalized gas production versus coal bulk density of the top and most developed coal seam based on the lowest coal density values in the well logs. The trend for the 6 wells shows that 5 of the wells increase in production with decreases in density. However, well W (blue block arrow) is an outlier with low production and low density. The correlation for this data is 0.96 with exclusion of well W.

Well W is a significant outlier with low values for density and production. Well W's behavior could possibly be due to the fact that it lies on the gradual back limb where the coal seams are at greater depths. With the exclusion of well W, the other 5 wells display a strong correlation of 0.96. Most of the wells in the study area have two to three perforated coal seam zones. Figure 22 is a plot of each well's average coal bulk density (from well logs over all perforated seams in the well) versus production. This correlation is less convincing at 0.46 with the exclusion of well W again. Figure 23 is a plot of the coal bulk density for the top coal seam from the multiattribute transform predictive volume. This result showed almost no correlation with production with an R^2 value of 0.21. Well W is one of the low producing wells that had extremely low density on this top layer. Wells W and Z are located on the gradual back limb of the fault-propagation fold and both are non-producers. The lower gradual back limb production could be due to the increased *in situ* stress at deeper depths causing more cleats and fractures to close thereby reducing the permeability. Well X is another low-producing well with low density that is located on the steep forelimb of the fold. Finally, Figure 24 is a plot of the average coal bulk densities (based on the multiattribute transform) from all the perforated coal seams versus production for the wells. The correlation for this plot is 0.52 with the exclusion of well X. Wells B and Z were not used in the transform training process. The multiattribute transform performed adequately in the prediction of the density values for wells B and Z, but the overall correlation was marginal.

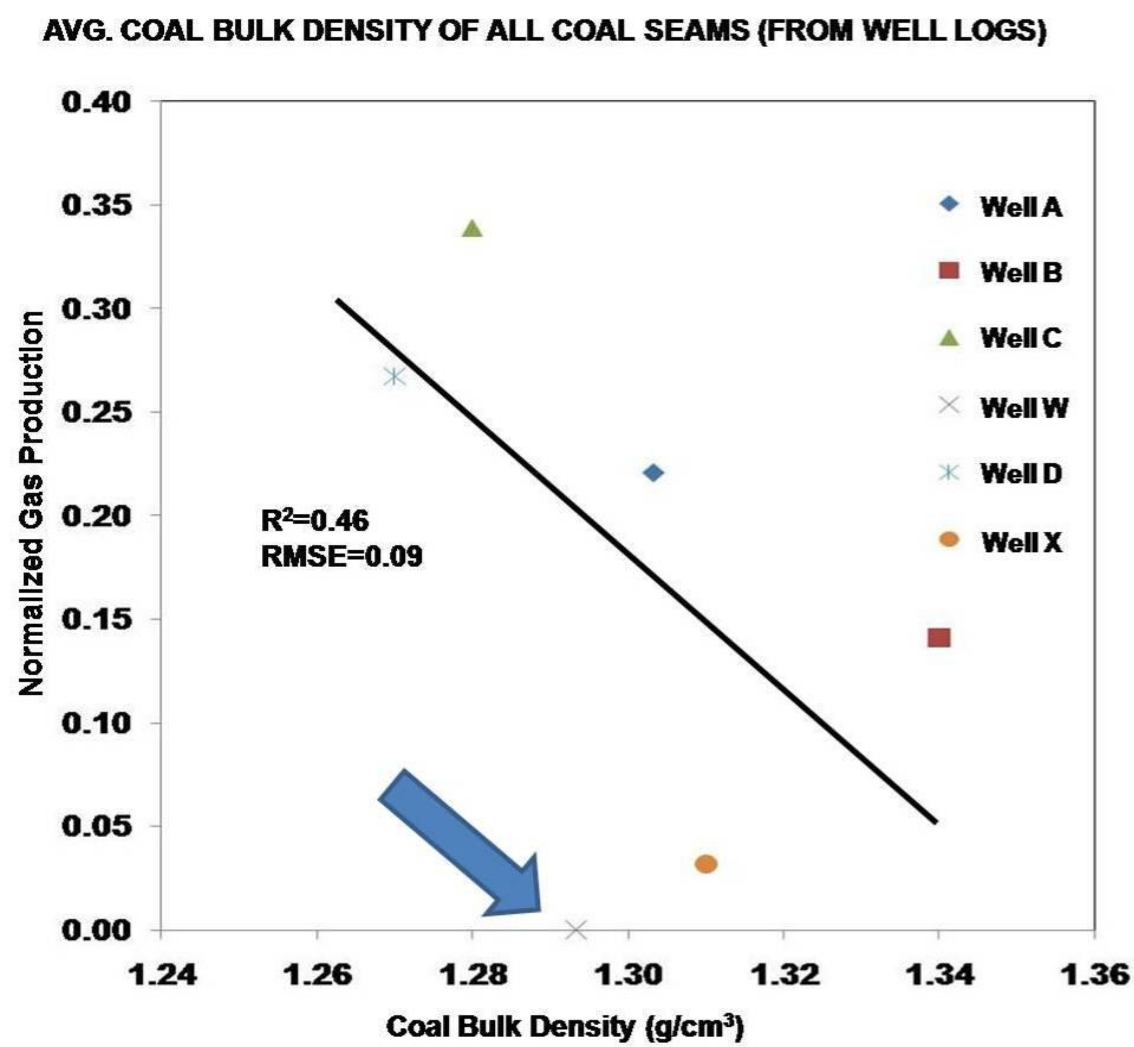

Figure 22. A plot of normalized gas production versus average coal bulk density of all perforated coal seams based on the lowest coal density values in the well logs. The general trend of low density and high production is still present but less evident with a correlation of 0.46 after excluding the anomalous behavior of well W (blue block arrow).

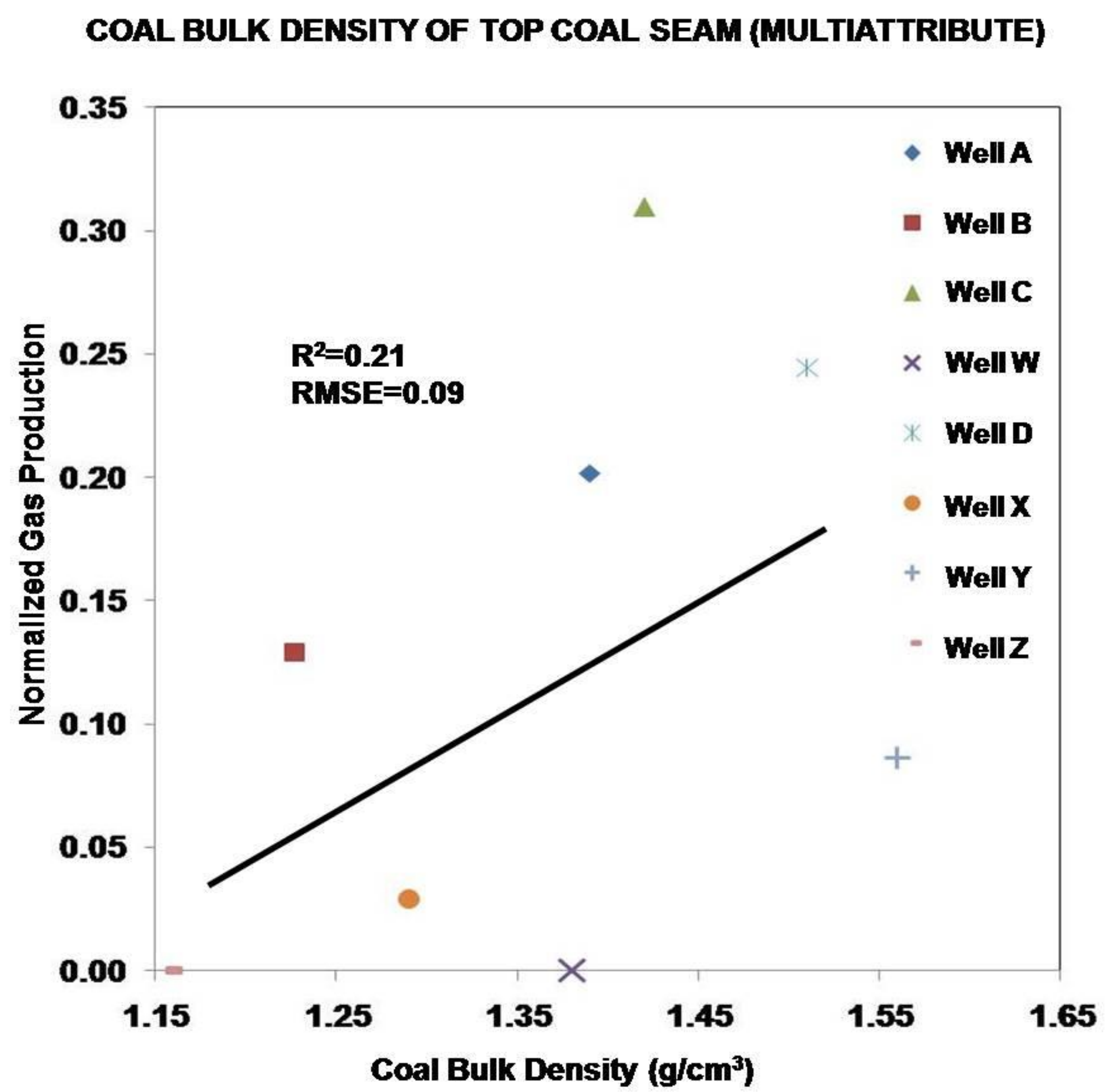

Figure 23. A plot of gas production versus the coal bulk density for the top coal seam in the seismic survey based on the multiattribute transform using colored acoustic impedance inversion, 54 Hz spectral magnitude component, and the square of the 124 Hz spectral magnitude component attributes. The poor correlation of 0.21 suggests no relationship between low density and higher production for the predicted density values from the top coal seam.

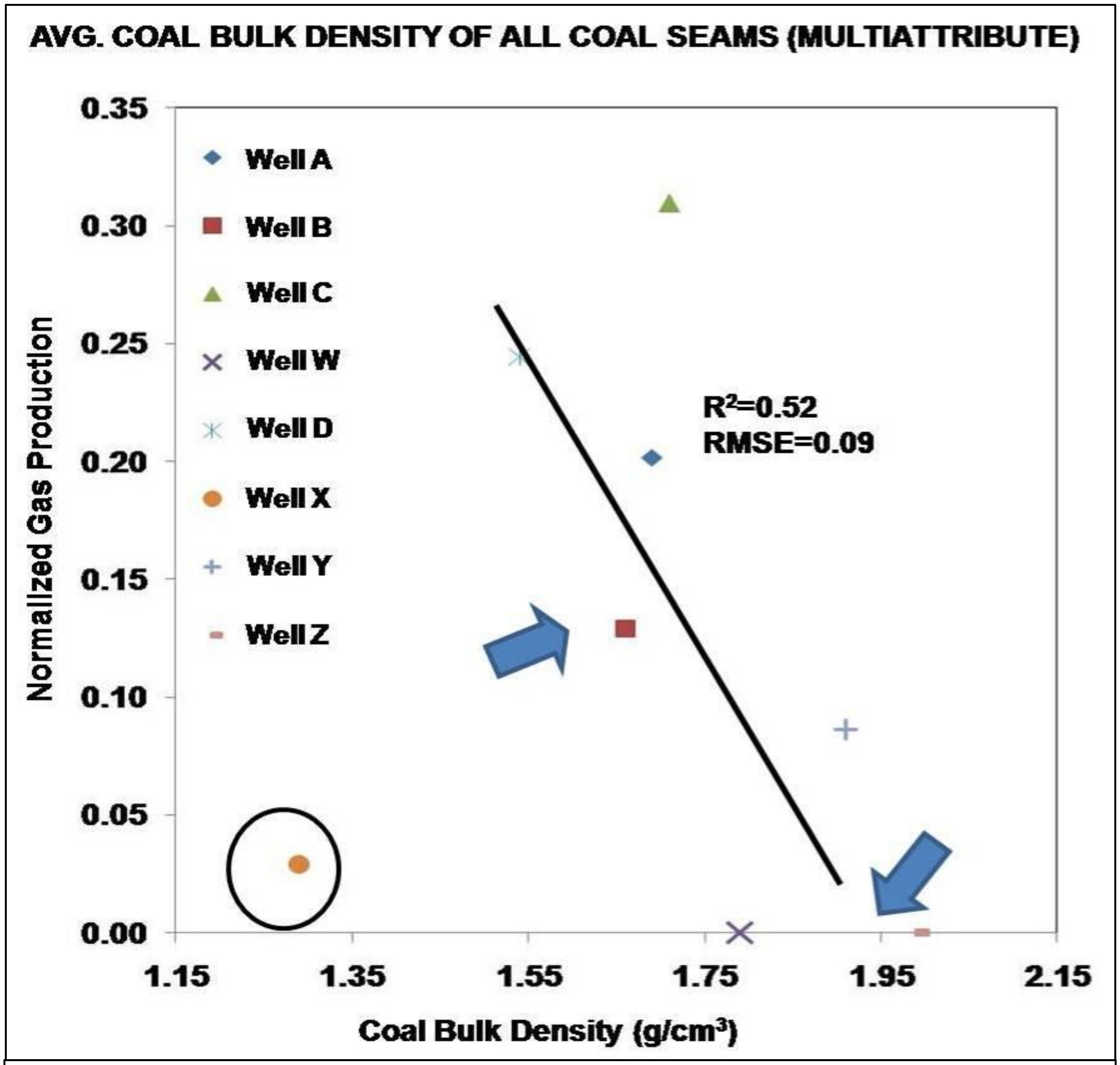

Figure 24. A plot of gas production versus the average coal bulk density for the wells in the seismic survey based on the multiattribute transform using colored acoustic impedance inversion, 54 Hz spectral magnitude component, and the square of the 124 Hz spectral magnitude component attributes. The block arrows are wells B and Z that were not used in the multiattribute training process. Their predicted average density values are in good correlation with their level of production. Well X (black circle) was an outlier whose low production was inconsistent with its extremely low average coal bulk density. With the exclusion of well X, the correlation was 0.52.

Figure 25 shows a vertical seismic slice from well A's location as viewed with the predictive density volume (density values above 1.9 g/cm^3 made transparent) co-rendered with the most-positive curvature volume.

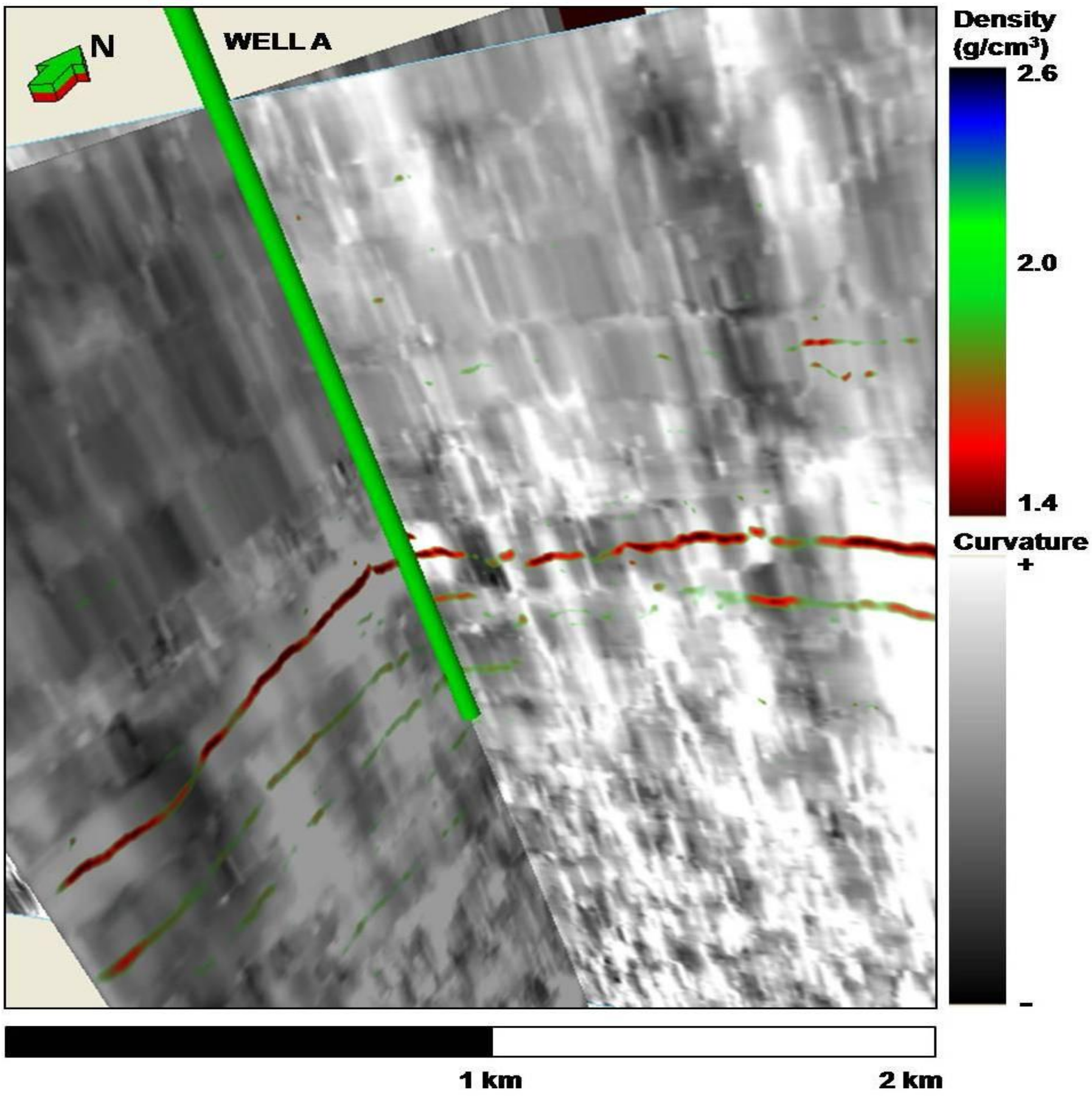

Figure 25. This view of well A shows the predicted density overlain on the most-positive curvature volume. Density values above 1.9 g/cm^3 have been made transparent. This view shows the multiple low density coal layers (in red and green) accessed by the wellbore. These layers are suspected to be rich in organic content, contributing to well A's high gas production.

VII. Structural Elements

A. Stress

Using image logs from wells in the survey area and borehole breakouts, Johnson et al. (2002) determined the maximum horizontal stress, $\sigma_{H\text{-}Max}$, of the survey area to be northeast. Hillis et al. (1999) reached similar results in eastern Australia for $\sigma_{H\text{-}Max}$ by observing fracture orientations with a digital downhole compass during hydraulic fractures. Figure 26 is the maximum horizontal stress map for Australia from the World Stress Map database. Most of the $\sigma_{H\text{-}Max}$ measurements in Figure 26 are from hydraulic fracture measurements and overcoring analysis (Heidbach et al., 2008). A significant amount of error exists in estimation of $\sigma_{H\text{-}Max}$. Figure 27 is the Bowen Basin rose diagram of the World Stress Map data. Heidbach et al. (2008) report an average standard deviation among the $\sigma_{H\text{-}Max}$ azimuthal measurements of 13.8˚. The rose diagram is a representation of 37 separate pairs of $\sigma_{H\text{-}Max}$ azimuth and magnitude measurements. The World Stress Map data suggests $\sigma_{H\text{-}Max}$ is north-northeast.

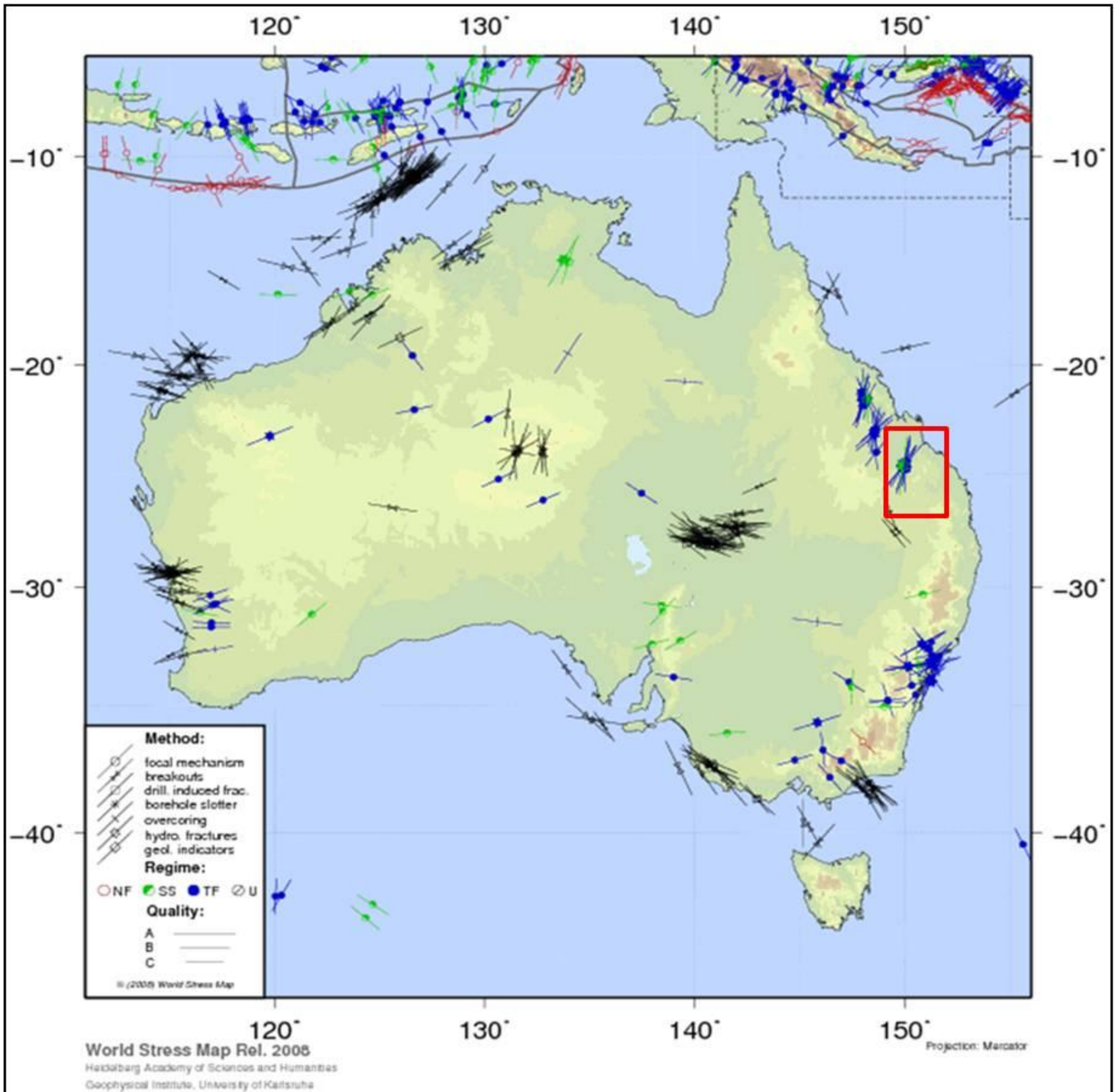

Figure 26. The map of maximum horizontal stress distributions in Australia. The red box indicates the area of interest for this study. Most of the $\sigma_{H\text{-}Max}$ measurements in the study area are from hydraulic fracture measurements and overcoring analysis (Modified after Heidbach et al., 2008).

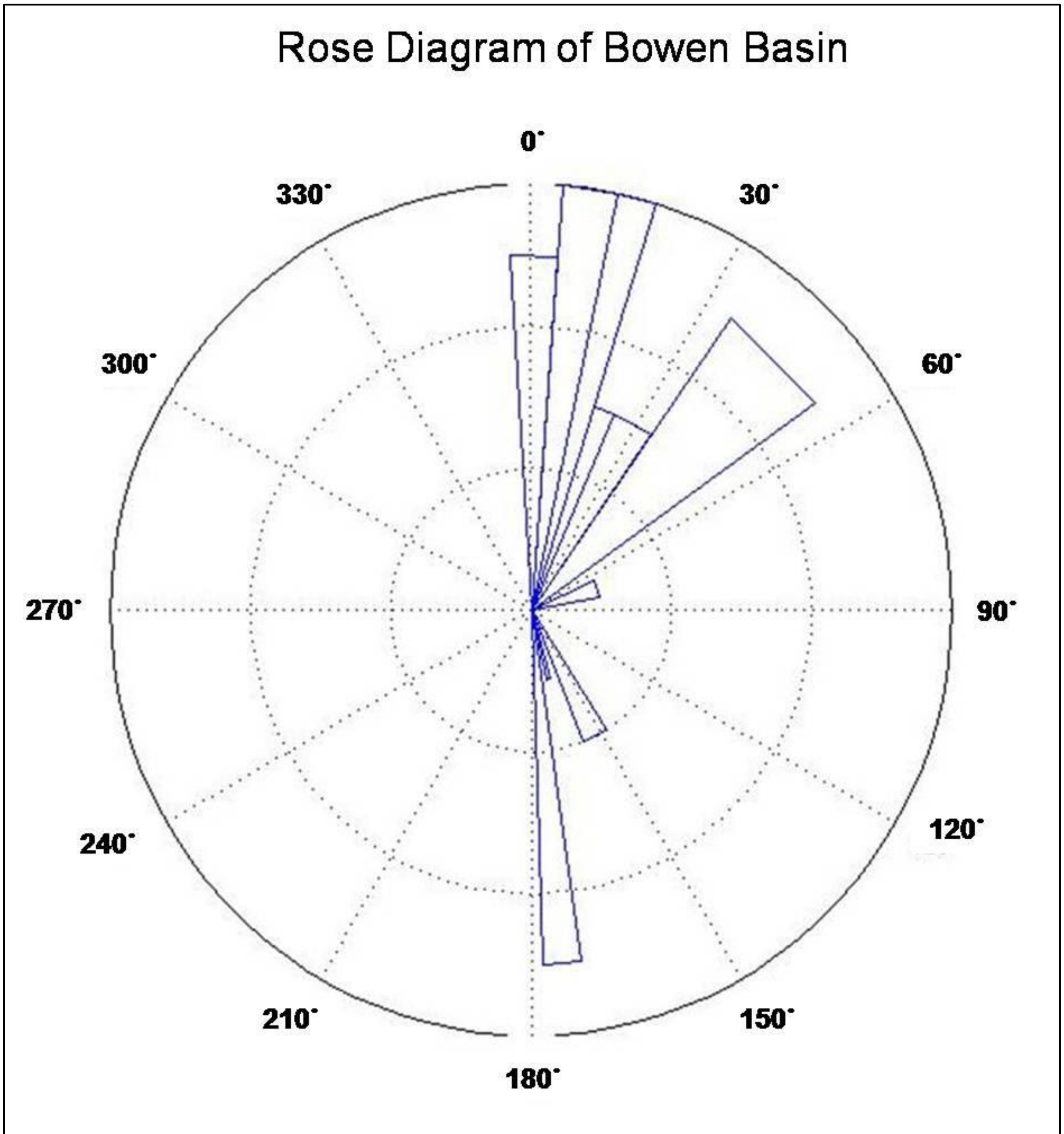

Figure 27. The rose diagram of the Bowen Basin from the World Stress Map database reveals a $\sigma_{H\text{-}Max}$ direction that is north to northeast. The average standard deviation of the azimuthal measurements is 13.8˚.

Cleats and fractures that are aligned parallel or near parallel to the maximum horizontal stress are more likely to be open and are likely to be the face cleats. Conversely, cleats and fractures aligned perpendicular to the maximum horizontal stress are more likely to be closed. Studies have shown that the intensity of *in situ* stress is as important as the stress direction in coalbed-methane reservoirs. *In situ* stress can be determined through bottomhole treating pressures or breakdown pressures. Enever et al. (1994) and Johnson et al. (2002) both mention that lower *in situ* stress states were correlated to high gas production in coal seams.

In most cleat formation hypotheses, exogenetic formation is one of the main sources of cleat formation (Ammosov and Eremin, 1960). Exogenetic cleats are formed from paleotectonic stresses, neotectonic stresses, or a combination of both (Close, 1993). The Goondiwindi Event in the Middle to Late Triassic postdates deposition of the coal. This event was part of a westward propagating thrust system (Korsch, 2004) that caused the fault propagation fold in our 3D seismic survey. Inferring from the geometry of the fault propagation fold, this major event would have represented a maximum horizontal paleostress oriented in a westward direction. Close (1993) notes that face and butt cleats often strike perpendicular and parallel, respectively, to major fold axes. Thus, the face and butt cleat orientations could be expected to be oriented east-west and north-south, respectively, if exogenetic cleats formed from the Goondiwindi Event. Today's stress systems in central and eastern Australia are between reverse stress and strike-slip, varying from location to location. Hillis et al. (1999)

point out that 80% of their data indicate a reverse fault condition and 17% indicate a strike-slip condition in the uppermost kilometer of crust in the Bowen Basin. The reverse fault condition is defined as ($\sigma_H > \sigma_h > \sigma_v$), where σ_H is the maximum horizontal stress, σ_h is the minimum horizontal stress, and σ_v is the overburden stress. The strike-slip fault condition is defined as a condition in which $\sigma_H > \sigma_v > \sigma_h$. Coblentz et al. (1995) suggest that the maximum horizontal stress direction in continental Australia is primarily controlled by collisional boundary forces acting along the Papua New Guinea boundary (Figure 28).

B. Curvature

Murray (1968) applied correlation of oil production to structural curvature concepts in the Bakken Formation. Nelson (2001) shows through outcrop and numerical methods that flexure-related fractures will be greatest at the location of maximum curvature. Volumetric curvature seismic attributes gauge the lateral variability in dip magnitude and dip azimuth (Mai et al., 2009). Curvature in three dimensions represents the values of the radii of two orthogonal circles fit tangent to a surface. Since curvature, k, is equal to the reciprocal of the radius of curvature for these circles, k_{min} represents the circle that fits tangent to the

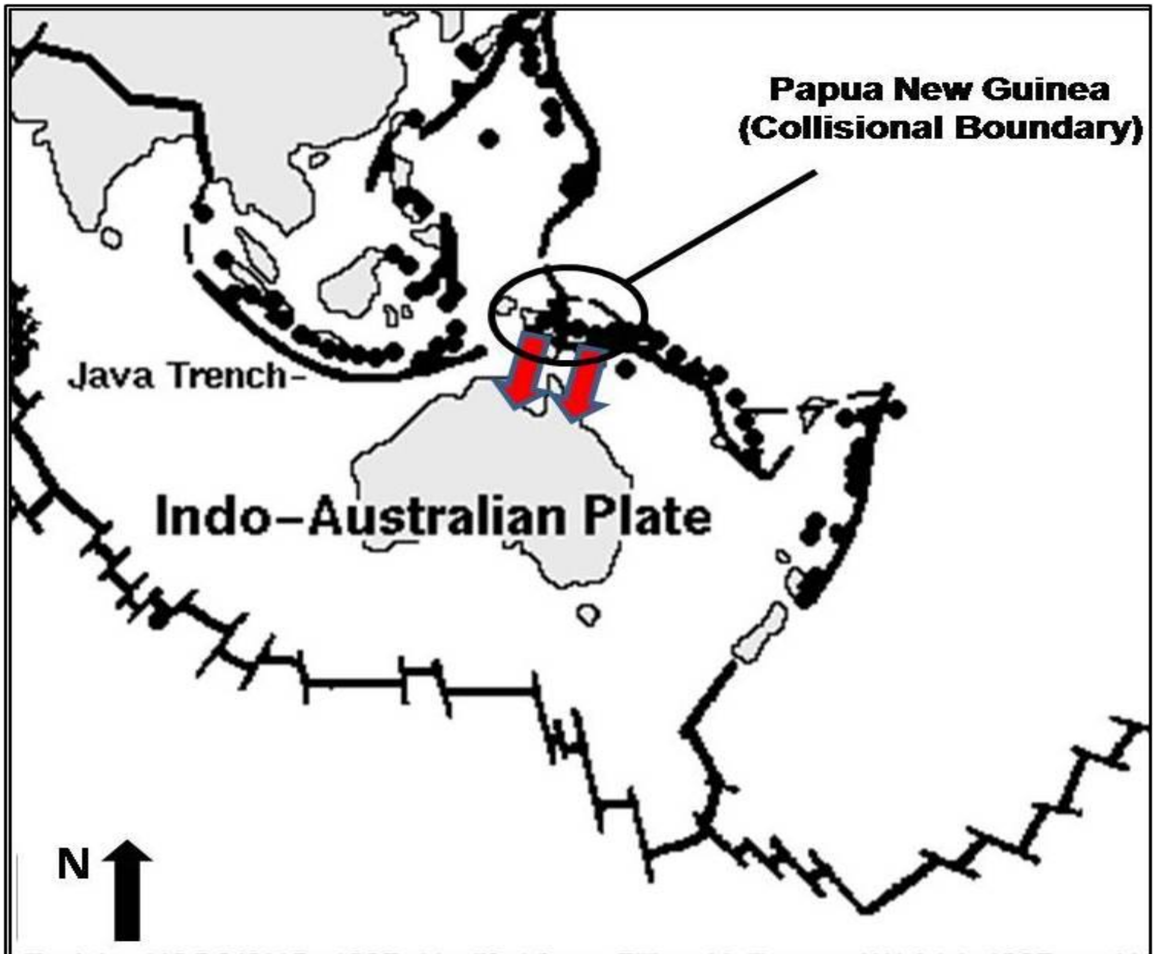

Figure 28. This tectonic plate map of the Indo-Australian plate shows the Papua New Guinea boundary as the source of today's stress in continental Australia according to models proposed by Coblentz et al. (1995). (Modified after USGS, 2010)

surface with the largest radius and k_{max} is the other circle tangent to the surface with the smallest radius (Chopra and Marfurt, 2007). Figure 29 provides a visualization of the relationship between curvature and geologic features in a 3D reference frame.

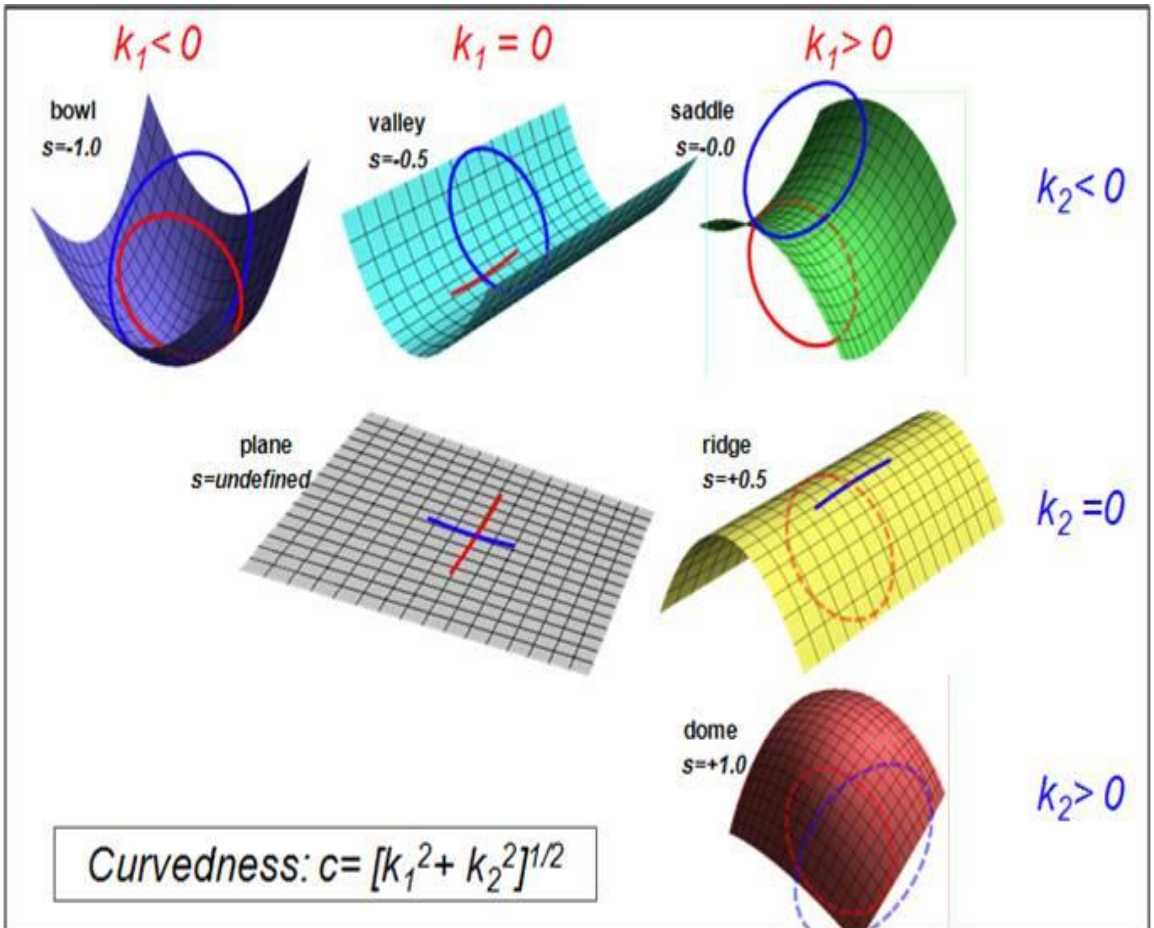

Figure 29. This figure defines 3D quadratic shapes in terms of most-positive and most-negative principal curvatures, k_1 and k_2. Bowl features have negative curvature values for k_1 and k_2, while dome features have positive curvature values for k_1 and k_2, while for a plane, both k_1 and k_2 have values of zero. The shape index, *s*, is shown for each of the five basic shapes (After Mai, 2010).

The mathematical calculation of curvature from an interpreted surface requires fitting a quadratic surface, $z(x,y)$, to a window of data points. The resulting principal curvatures are computed from first and second derivatives of these picks. *Volumetric* structural curvature is similar, but replaces the first derivative calculations with volumetric estimates of the inline and crossline dip (Marfurt, 2010). Chopra et al. (2009) point out that the most positive and most negative principal curvatures are the most effective in "mapping subtle flexures and folds associated with fractures in deformed strata." In *volumetric* amplitude or impedance curvature calculations, the first derivative calculations are replaced by volumetric estimates of the inline and crossline gradients as directional measures of amplitude variability (Chopra and Marfurt, 2007).

Curvedness provides a measure of the intensity of structural deformation at a given point. Roberts (2001) define the curvedness, *c*, of a surface as:

$$c = [(k_1^2 + k_2^2)/2]^{\frac{1}{2}}, \tag{5}$$

where k_1 is the maximum principal curvature and the minimum principal curvature is k_2. These principal curvatures measure the maximum and minimum bending of the surface at each point (Lisle, 1994). Roberts (2001) defines the shape index, *s*, as:

$$s = \frac{2}{\pi} tan^{-1}\left[\left(\frac{k_2 + k_1}{k_2 - k_1}\right)\right]. \tag{6}$$

The result of the shape index is a seismic attribute volume whose amplitudes correspond to shapes, where the shape index of a dome is 1.0, a ridge is 0.5, a saddle is 0.0, a valley is -0.5, and a bowl is -1.0. When the shape index is co-rendered in a seismic display with curvedness, high curvedness values that correspond with ridge and valley shape indices are directly related to lineaments (Chopra et al., 2009).

C. Curvature Case Study

Marfurt and Mai (2009) suggest that the ridge component is better to use in compressional regimes, and the valley component is better to apply in extensional environments. Taking this concept, I first consider the most-positive principal *structural* curvature attribute to illuminate anticlinal features that may be highlighted as result of the thrust system in this 3D seismic survey. Figure 30 is the most-positive structural curvature attribute with high red curvature values indicating strong high-amplitude lineaments.

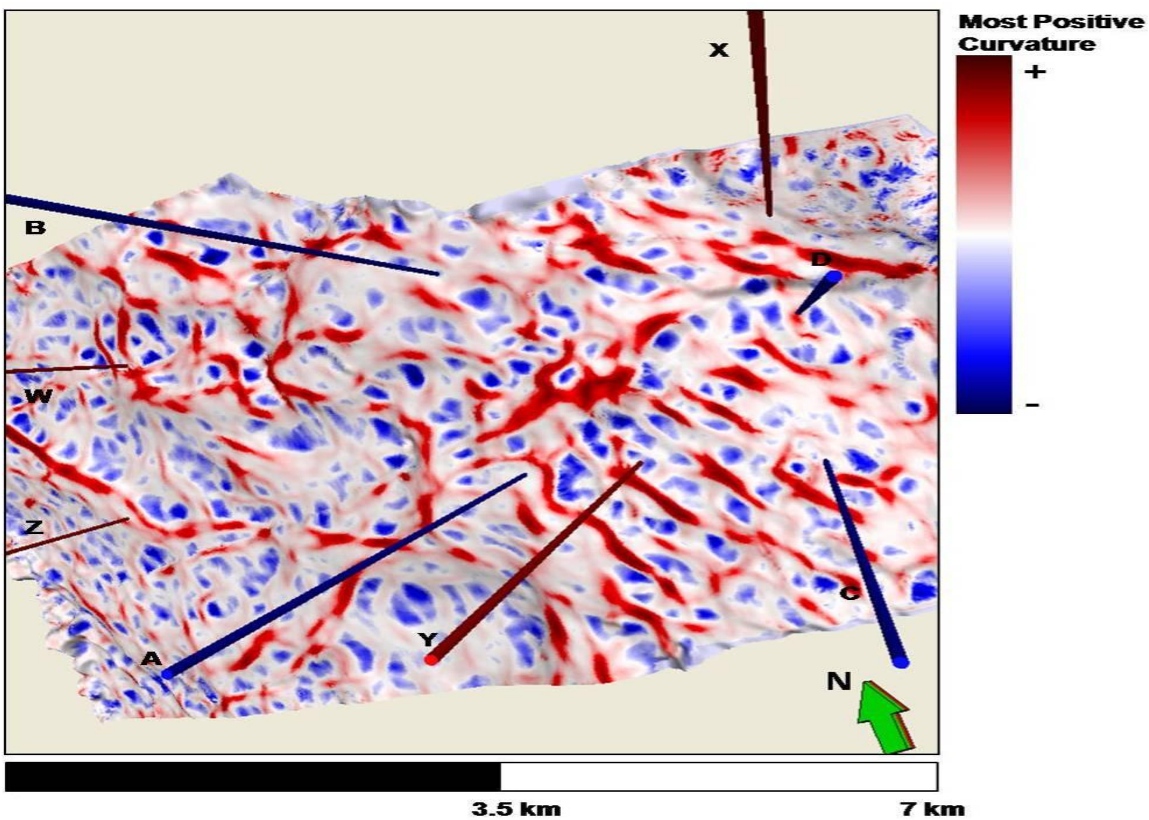

Figure 30. This view is of the top coal seam through the most positive structural curvature volume. High values (red) indicate anticlinal features or ridge-like lineaments. The wells under examination reveal that lower producing wells (red wellbores) have strong northwest directed structural features nearby.

This figure shows that the lower producing wells X and Y have a single, strong northwest structural lineament near the wellbore. Considering that $\sigma_{H\text{-}Max}$ is oriented to the northeast, this curvature evidence suggests that single structural lineaments near a wellbore or proposed drilling location oriented perpendicular to $\sigma_{H\text{-}Max}$ may be counter-productive to higher gas rates. Figure 31 shows the most-positive amplitude curvature attribute.

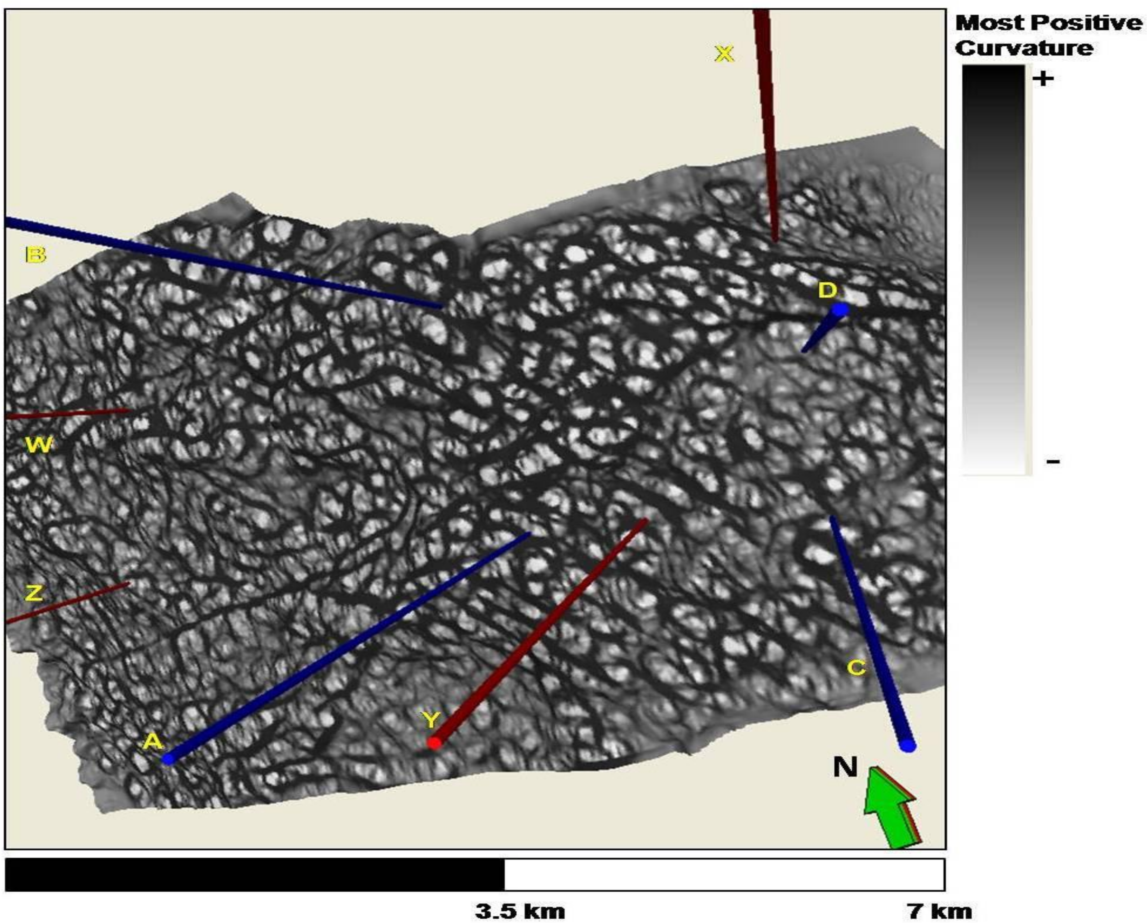

Figure 31. View of the top coal seam through the most positive *amplitude* curvature volume. High values (black) indicate locally high reflectivity lineaments. The high producer (well A) shows strong most positive amplitude curvature trends from orthogonal directions leading to the wellbore. The surrounding low producers (red wellbores) do not show this same trend.

This attribute illustrates a lineament network of strong most-positive curvature events that intersect the high-producing well A from orthogonal directions. The surrounding lower-producing wells do not have these strong lineament trends leading to their wellbores. These trends help to illustrate subtle lateral variations in amplitude that can provide clues to geologic changes such as lithology or thickness. I also computed the most positive amplitude curvature using the colored acoustic impedance inversion as the input volume instead of the raw seismic data. The result is an amplitude curvature volume whose high curvature values correspond to lineaments of high impedance and are mathematically independent of structural curvatures. The result reveals that high acoustic impedance lineaments correlated closely with low-producing wells. Likewise, high producers show fewer high impedance trends in close proximity of the wellbores. Figure 32 is the most positive acoustic impedance curvature volume.

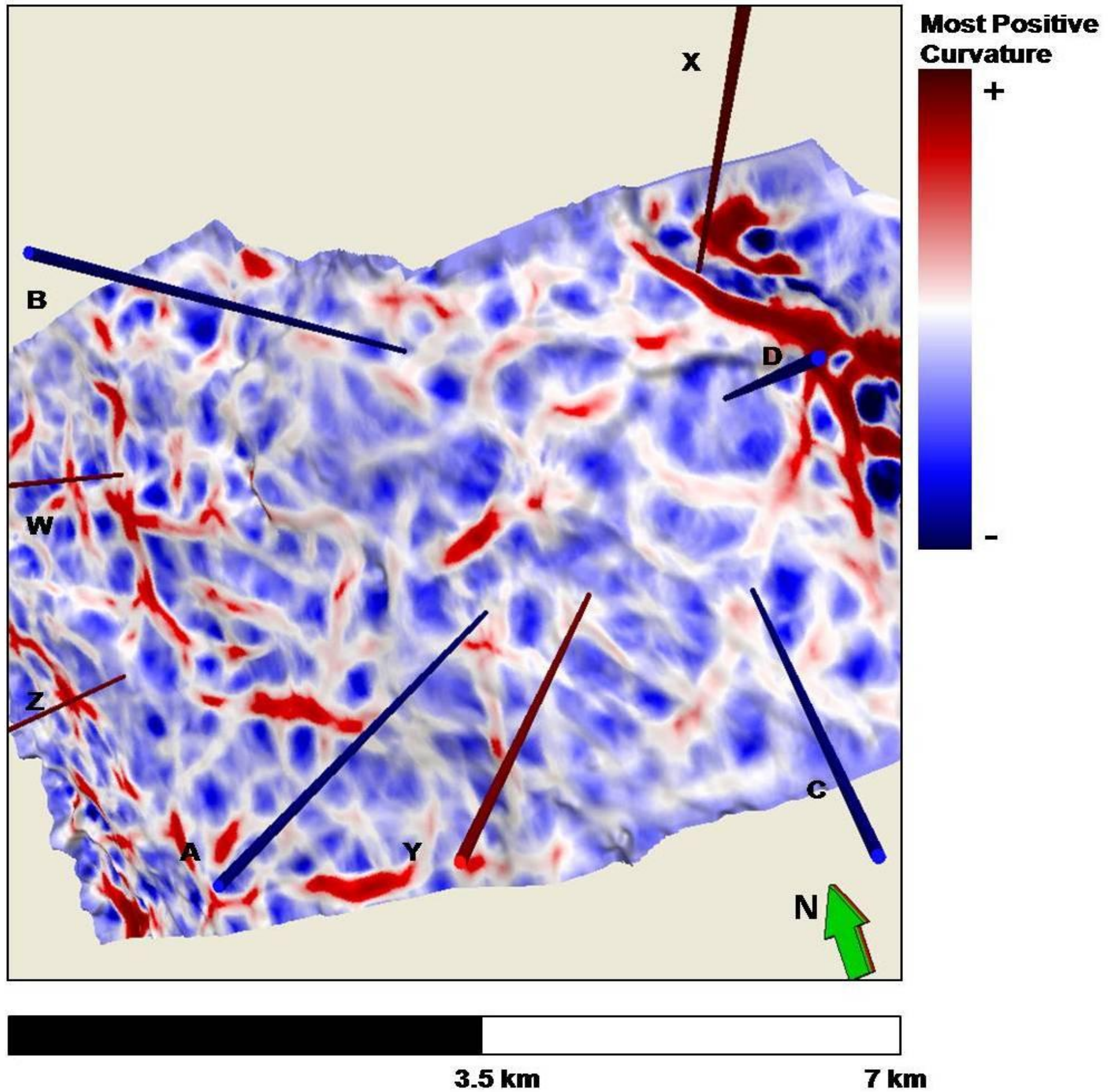

Figure 32. View of the top coal seam through the most positive acoustic impedance curvature volume. High values (red) indicate locally high acoustic impedance lineaments. The low producers (red wellbores) show strong most positive high impedance, high curvature lineaments in the vicinities of the wellbores.

The shape index co-rendered with curvedness (Figure 33) provides additional insight into the topography of the top of the coal seam. Figure 33 shows the areas of high curvedness and intense structural deformation that correspond with different shapes, most notably ridge features associated with compressive stress regimes.

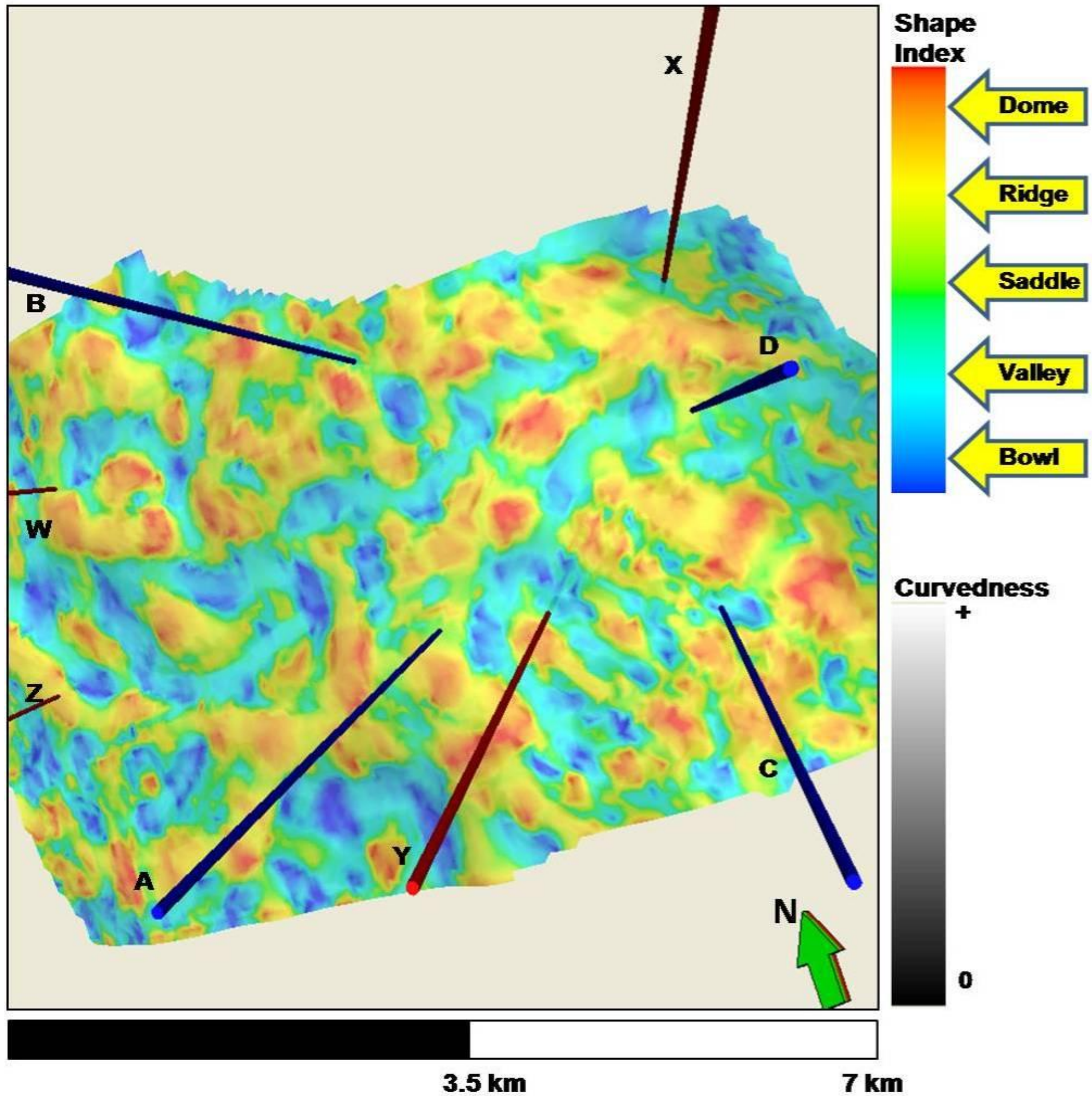

Figure 33. The top coal seam displayed as the shape index co-rendered with the curvedness. The areas with greater curvedness and more structural deformation appear with white undertones.

Figure 34 shows the acoustic impedance values less than 15,000 ft/s*g/cm^3 overlain on the shape index horizon slice. This image suggests that pockets of lower acoustic impedance coals in this survey coincide with areas with a concentration of dome features. The lower acoustic impedance values in the areas with a significant amount of dome features could be the result of more open cleats and fractures at these points of high flexure that result in less dense, lower velocity coals.

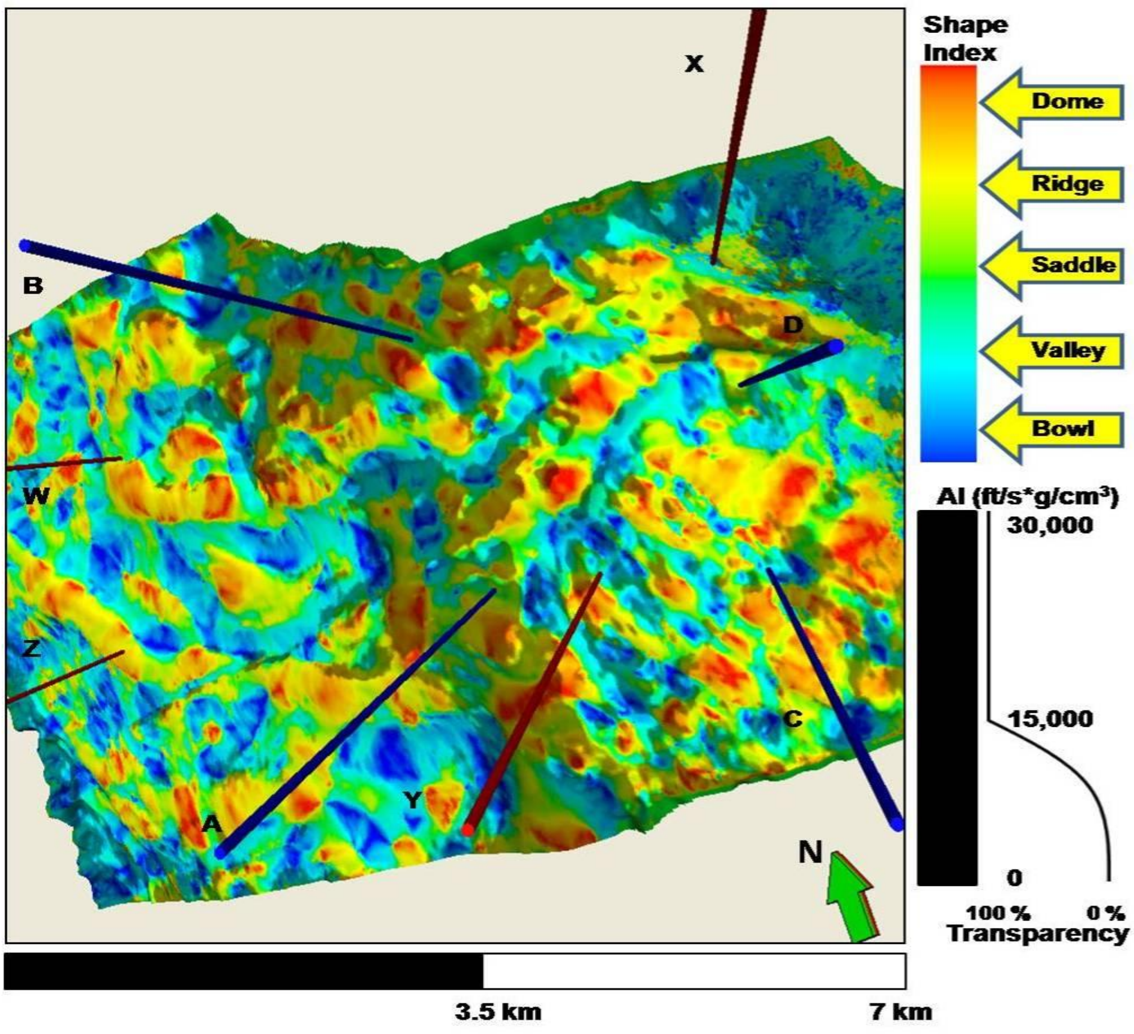

Figure 34. The top coal seam through the shape index with dark geobody patches being acoustic impedance values less than 15,000 ft/s*g/cm^3. This image shows a correlation between low acoustic impedance values and areas with the highest concentration of dome features covering a strongly-bending portion of the fault propagation fold.

D. 3D Rose Diagrams

Estimation of face and butt cleat orientation is critical to planning wellbore trajectory and completion procedures. Since the resolution of my seismic survey is limited to about 8 m, I need to use an indirect approach in determining the orientation of cleats. Multiple studies have determined that coal butt and face cleats, having apertures on the order of millimeters, are correlated to the regional fracture geometry. Nelson (2001) found that regional fractures usually parallel cleat directions, with face cleats corresponding to the systematic regional fracture set and butt cleats the non-systematic regional fracture set. Grout (1991) notes that cleats in the southern Piceance basin correlate to fractures in overlying clastic rocks.

I determine the fracture set orientations seismically through the generation of 3D rose diagrams. In this process, a seismic volume is binned in even squares of 250 m x 250 m. Then, the magnitude of a given rose petal at a single horizon is defined by the summed and scaled ridge or valley component of curvature values within a bin. The strike direction of the rose petal is defined by the value for the strike of minimum curvature, which is the axis of the folding plane. More details for this process are documented in Chopra et al. (2009).

E. 3D Rose Diagrams Case Study

I investigate the fracture orientations near the top coal horizon with the 3D rose diagrams. I expect that better producing wells will show a strong presence of fractures oriented parallel to $\sigma_{H\text{-}Max}$. Figure 35 is the top coal surface with the

3D rose diagrams overlain at the well locations. This image reveals that the higher producing wells A and D show a strong bi-directional trend, suggesting that contributions from both systematic and non-systematic fracture sets or a strong presence of face and butt cleats may be contributing to the wells' deliverability.

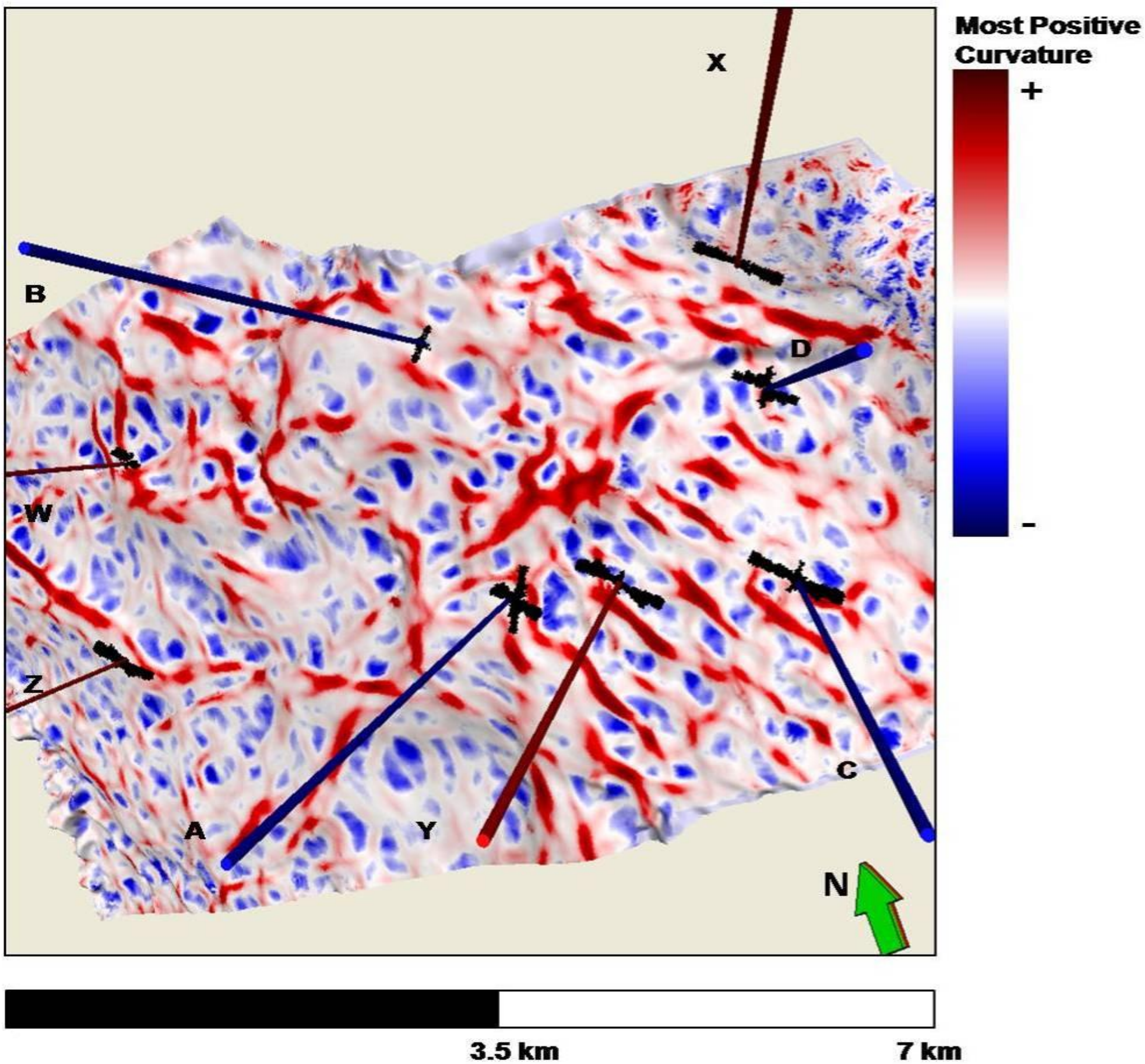

Figure 35. Map view of the top coal seam showing the 3D rose diagrams at the respective well locations. The rose diagrams show strong bi-directional trends at higher producing wells A and D, and lower producing wells W, X, and Y show a more uni-directional trend.

Furthermore, rose diagrams of the lower producing wells W, X, and Y show a more uni-directional trend. Highlighting the complexity of this reservoir, Figure 35 shows well C as a higher producing well with more of a single fracture trend; however, this well has a very high cumulative coal thickness (9.3 m) at the top coal seam.

F. Azimuthal Anisotropy

Azimuthal pre-stack gathers consist of subgroupings of traces from a common midpoint gather. These subgroupings are based on azimuths from the source to receiver. In this study area, the azimuthal gathers were separated into azimuths of 0-45˚, 45-90˚, 90-135˚, and 135-180˚, and azimuthal normal moveout corrections were applied.

Lynn (2004) explains that "aligned ordered heterogeneities" (cleats in this study) "can cause azimuthal anisotropy". Lynn (2004) defines azimuthal anisotropy as variations of traveltimes and amplitudes that show a 90˚ variation with azimuth between fast-to-slow directions. In P-wave azimuthal anisotropy, the fast direction should align with the direction parallel to maximum horizontal stress and the systematic regional fracture set. Likewise, the slow direction should be perpendicular to the dominant fracture set. Figure 36 provides a more physical explanation of this fast and slow direction phenomenon.

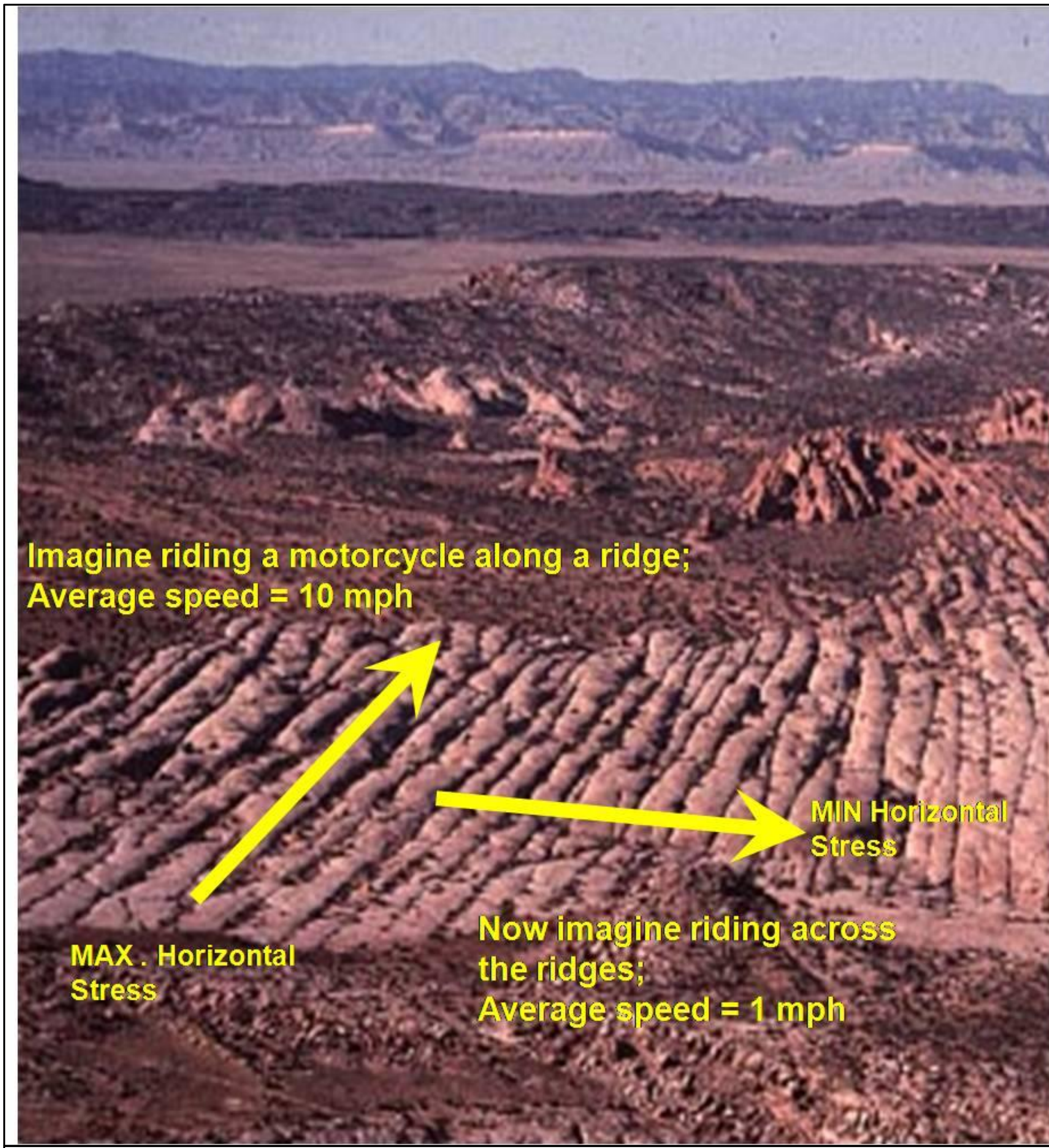

Figure 36. The arrows depict the theoretical travel paths of P-waves parallel and perpendicular to the maximum and minimum horizontal stress. One can see how the P-wave traveling in the minimum horizontal stress direction could be slowed down by aligned ordered heterogeneities such as cleats (Modified after Lynn and Lynn, 2008).

G. Azimuthal Anisotropy Case Study

For this analysis, I stacked the azimuthal gathers and then applied a bandlimited acoustic impedance inversion to the post-stack azimuthal data.

Figures 37 and 38 are the bandlimited inversion images of the top of the coal seam for the 0-45˚ and 45-90˚ post-stack azimuthal volumes. The 0-45˚ bandlimited volume (Figure 37) showed the highest range of acoustic impedance values and the highest mean value (33,705 ft/s* g/cm^3) of all the azimuths.

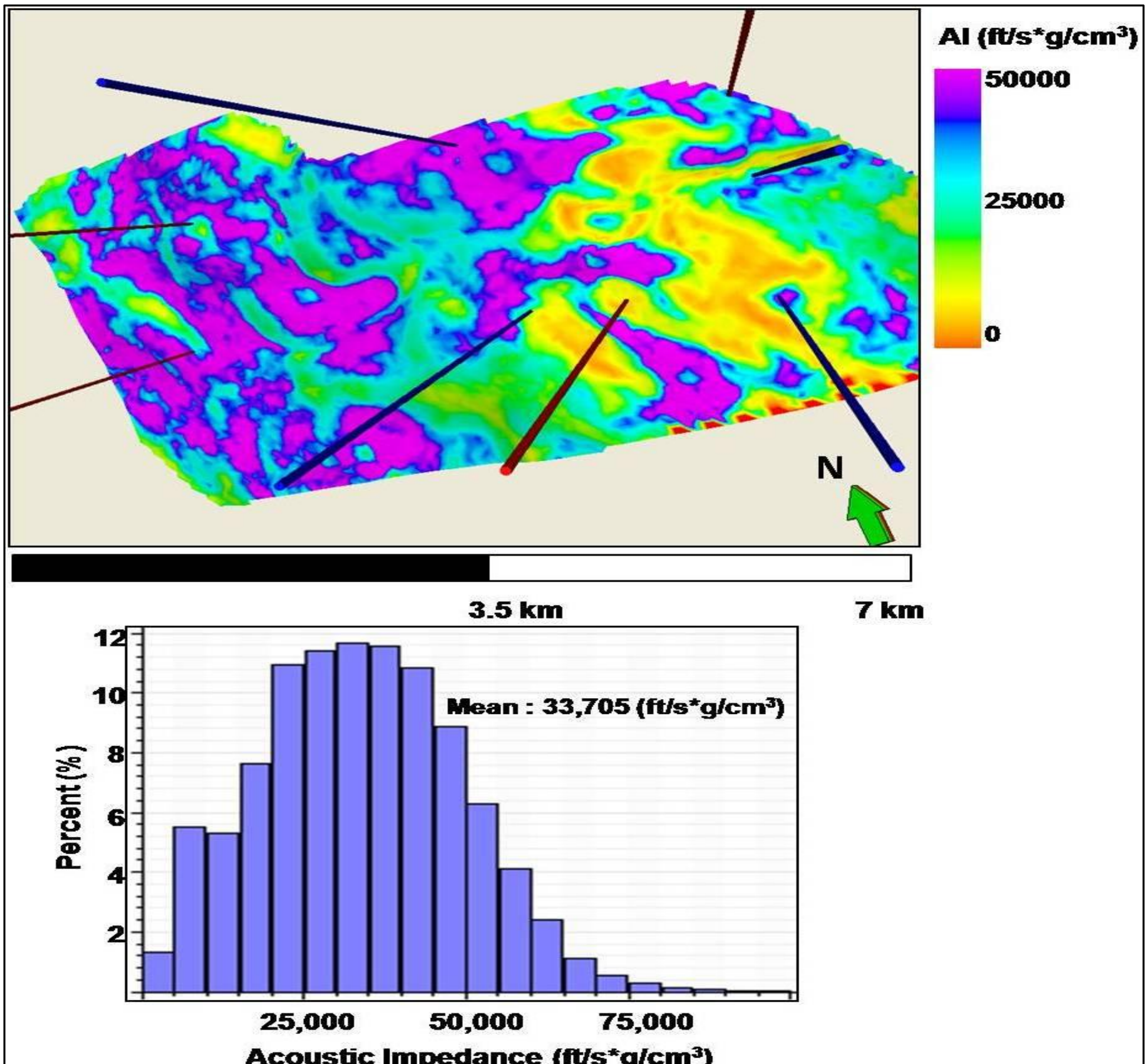

Figure 37. The bandlimited acoustic impedance from the top of the coal seam. This acoustic impedance volume is a product of stacked azimuthal gathers for azimuths 0-45˚. The acoustic impedance values are greatest in this direction. I interpret the higher values in this direction to be the result of faster velocities along the strike of the dominant cleat direction.

The 45-90˚ bandlimited volume (Figure 38) showed a lower range of acoustic impedance values and the lowest mean value (24,540 ft/s* g/cm^3) of the range of azimuths.

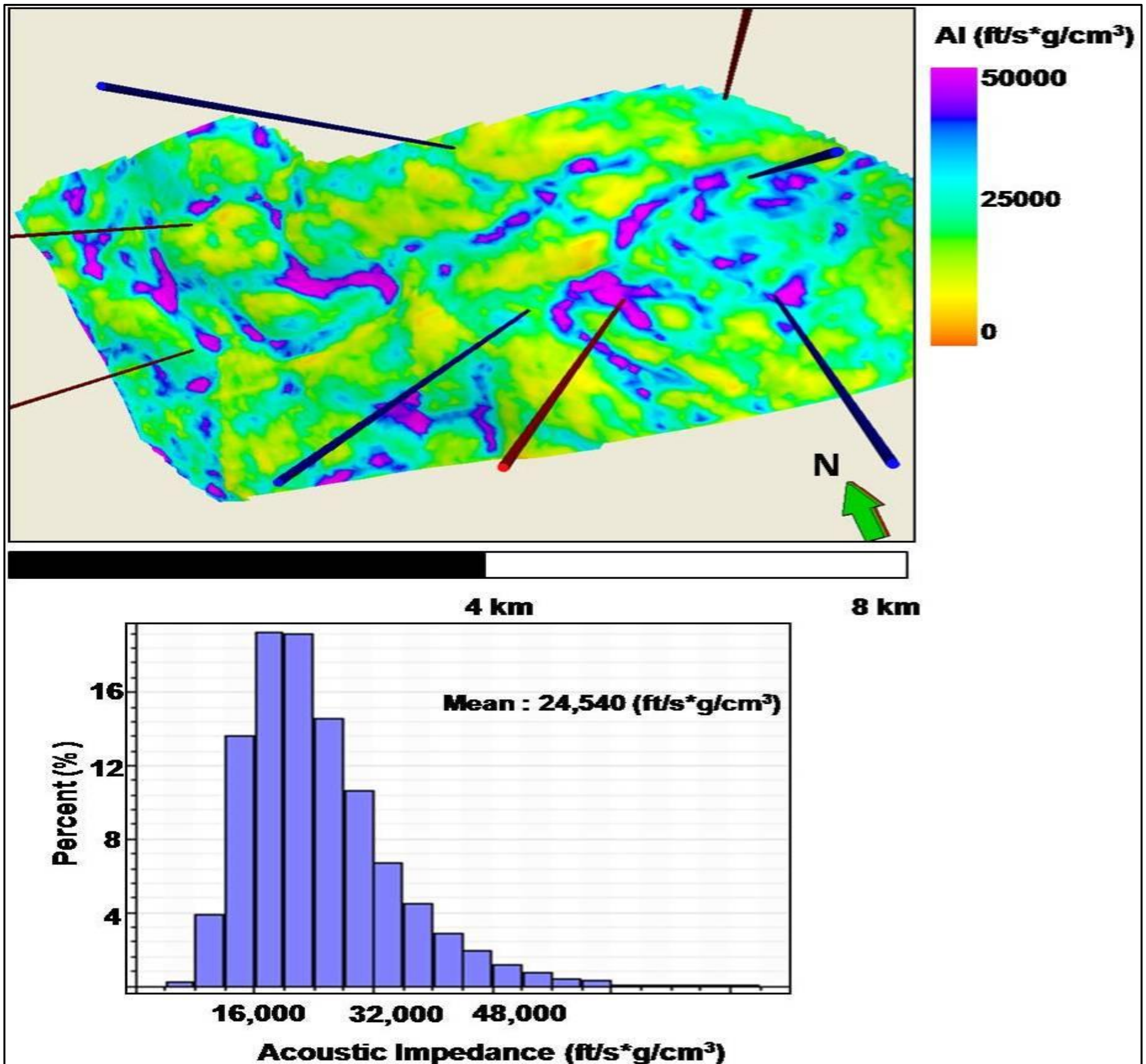

Figure 38. The bandlimited acoustic impedance from the top of the coal seam. This acoustic impedance volume is a product of stacked azimuthal gathers for azimuths 45-90˚. The acoustic impedance values are least in this direction.

The high values in the 0-45˚ azimuthal range are consistent with the fact that the maximum horizontal stress is oriented to the northeast. Since acoustic impedance is the product of density and velocity, I interpret the high acoustic impedance values in the northeast direction to be due to the fast velocities parallel to maximum horizontal stress. The lowest acoustic impedance values occurred between 45-90˚ azimuths when the P-waves propagate oblique to the two different fracture sets (face and butt cleats). Figure 39 is a depiction of the geometry associated with the P-wave encountering the cleat sets in this survey area.

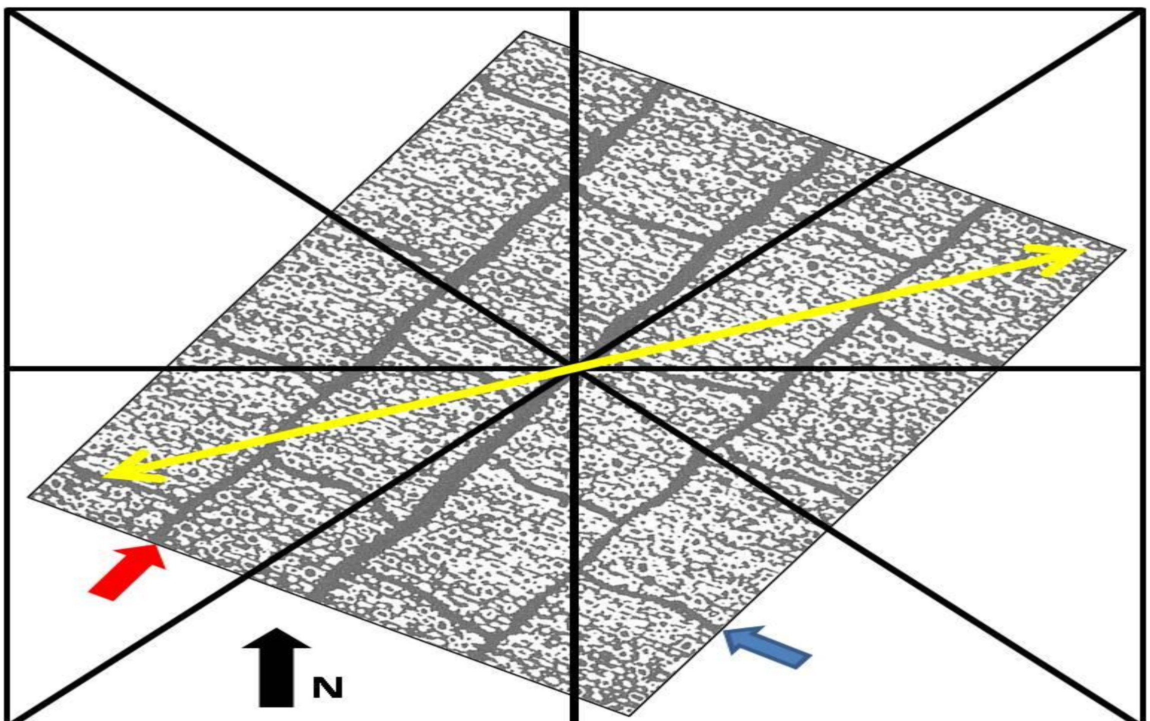

Figure 39. A depiction of the travel path of P-waves (yellow double arrow) that move in the slowest direction in this survey. The face cleats (red block arrow) are in the northeast direction (0-45˚ azimuth) aligned with maximum horizontal stress and corresponding with the highest mean value of acoustic impedance and fastest direction of P-wave travel. The blue block arrow corresponds to the butt cleat direction. Traveling at a 45-90˚ azimuth the yellow arrow encounters maximum fracture density in this example.

VIII. Conclusions

Ash content is linked to bulk density values and can be linked to gas generation with increasing coal rank. High bulk density can be an indicator of a less productive coal seam, such that density logs and density inversion can estimate the purity of the coal seams in the reservoir. Multiattribute transforms provide a means of predicting density values away from well control throughout the 3D seismic survey. In this study, low density values from well logs and high gas production rates are correlated in the top coal seam (R^2=0.96) between five wells in the study area. Additionally, dome and ridge features in the shape index correlated with low patches of density throughout the survey area. However, the predicted density values from the multiattribute transform displayed a poor correlation (R^2=0.21) with production rates when considering two blind wells in the survey area. This poor correlation is likely due to the extremely thin nature of the coals in the survey, making it difficult for seismic data and seismic attributes to predict a true representation of the layers below one quarter of a wavelength (approximately 7 m).

Integration of the *in situ* stress regime directions from image logs and borehole breakouts with seismic curvature attributes and 3D rose diagrams provide insight to varying production and cleat orientations. Wells with a nearby singular most-positive principal structural curvature lineament perpendicular to the maximum horizontal stress tend to be less productive. This lower gas rate level is due to fractures and cleats oriented perpendicular to $\sigma_{H\text{-}Max}$ having a propensity to closure. The amplitude curvature volume reveals high amplitude lineaments along the maximum and minimum horizontal stress directions leading to the wellbore of a high-producing well. In the amplitude curvature volume computed on acoustic impedance, high acoustic impedance lineaments correlate to low-producing wells throughout the survey. Higher producing wells have a bi-directional 3D rose diagram that suggests a strong existence of cleats in two directions (butt and face cleats) that enhance the permeability. The shape index shows patches of low acoustic impedance that fall within the areas of the survey with the strongest presence of dome features. These low acoustic impedance trends in areas with high-flexure dome shapes are indications of opening cleats and fractures that reduce the density and velocity of the coal.

Band limited acoustic impedance inversion of stacked azimuthal gathers provide some insight to the direction of faster P-wave velocity and face cleats. The direction with highest impedance values coincides with the maximum horizontal stress direction. The direction of lowest impedance values is oblique to both the maximum and minimum horizontal stress directions.

The azimuthal analysis, 3D rose diagram analysis, and seismic curvature and acoustic impedance analysis are extremely important elements of the analysis of coalbed-methane reservoirs. Similar to reservoirs throughout the world, coalbed-methane reservoirs are being seen in a new light with the proliferation of horizontal drilling. Horizontal drilling perpendicular to the face cleat direction is critical to optimizing production in these reservoirs. The aforementioned analysis methods provide a geophysical framework to approach this process of face cleat direction determination.

IX. Benefits of Solution

Australia is the world's second largest producer of coalbed-methane (Faiz, 2008). Numerous studies focus on seismic attributes and rock physics for coal beds in the San Juan Basin of New Mexico and other areas of the world. However, few seismic attribute studies have been conducted that correlate seismic attributes to production in Australia. I provide a synthesis of different geotechnical techniques available to a geologist or geophysicist to apply to a coalbed-methane reservoir to facilitate analysis of potential sweet spots. Further, I hope this study reveals that there is no single variable that allows for clarity of a good coalbed-methane prospect versus a poor prospect, but rather a complex set of criteria that must be considered.

X. Recommendations for Future Data Acquisition

I would recommend that the operator acquire multi-component seismic data in future coalbed-methane reservoir seismic surveys. The use of shear wave data analysis allows for enhanced resolution of fast and slow directions due to shear wave birefringence. Moreover, the operator should consider running image logs and taking core samples from more well locations. These tools and techniques are more expensive, but the image logs and core allow for more reservoir clarity and understanding throughout the gas field. Microseismic data should be considered during hydraulic fractures to attempt to confirm cleat directions by assessing the predominant fracture propagation direction. Finally, the operator should acquire more dipole sonic logs. Shear wave sonic logs allow for elastic impedance inversion which can facilitate an analysis of Lame' elastic rock parameters. Analysis of these rock properties can allow for a better understanding of the areas of less competent rock that might be more prone to fracturing and enhanced permeability.

References

American Geological Institute Website, 2009, Glossary of Geology, http://www.agiweb.org/, accessed 21 February 2009.

Ammosov, I.I., and I.V. Eremin, 1963, Fracturing in coal (translated from Russian): Office of Technical Services, Washington D.C.

Ayers, W.B., Jr., 2002, Coalbed gas systems, resources, and production and review of contrasting cases from the San Juan and Powder River Basins: AAPG Bulletin, **86**, 1853-1890.

Bose, S., 2010, Personal Correspondence at the University of Oklahoma, Spring 2010.

Boyer, C.M., II, 1989, The coalbed methane resource and the mechanisms of gas production: GRI Topical Report, GRI-89/0266.

CGG Veritas, 2007, Hampson-Russell Software Theory Documentation - Emerge Theory: CE8 version.

Chopra, S., and K.J. Marfurt, 2007, Seismic Attributes for Prospect Identification and Reservoir Characterization: Society of Exploration Geophysicists.

Chopra, S., K.J. Marfurt, and H.T. Mai, 2009, Using 3D Rose diagrams for correlation of seismic fracture lineaments with similar lineaments from attributes and well log data: 79th Annual International Meeting, SEG, Expanded Abstracts, 3574-3578.

Close, J.C., 1993, Natural fractures in coal, *in* B.E. Law and D.D. Rice, eds., AAPG Studies in Geology, **38**,119-132.

Coblentz, D.D., M. Sandiford, R.M. Richardson, S. Zhou, and R.R. Hillis, 1995, The origins of the intraplate stress field in continental Australia: Earth and Planetary Science Letters, **133**, 299-309.

Crosdale, P.J., 2007, Analytical Report: Petrographic Analysis and Proximate and Ultimate Analysis of Coals C2A, C2B, C3A, and C3B: Energy Resources Consulting PTY Ltd, Queensland, Australia.

Draper, N.R., and H. Smith, 1966, Applied regression analysis: John Wiley & Sons, Inc.

Enever, J.R., C.I. Pattison, R.H. McWatters, and I.H. Clark, 1994, The relationship between *in situ* stress and reservoir permeability as a component in developing an exploration strategy for coalbed methane in Australia: Proceedings of the SPE/ISRM International Conference August 1994.

Faiz, M., 2008, Coal bed methane in Australia: Diverse gas resources and geological settings of the major producing fields: International Geological Congress, Abstract.

Grout, M.A., 1991, Cleats in coalbeds of southern Piceance basin, Colorado - correlation with regional and local fracture sets in associated clastic rocks, *in* S.D. Schowchow, D.K. Murray and M.F. Fahy, eds., Coalbed methane of western North America: Rocky Mountain Association of Geologists, 35-47.

Hampson, D.P., J.S. Schuelke, and J.A. Quirein, 2001, Use of multiattribute transforms to predict log properties from seismic data: Geophysics, **66**, 220-236.

Heidbach, O., M. Tingay, A. Barth, J. Reinecker, D. Kurfeβ, and B. Muller, 2008, The World Stress Map database release 2008 doi:10.1594 /GFZ. WSM.Rel2008.

Hillis,R.R., J.R. Enever, and S.D. Reynolds, 1999, *In situ* stress field of eastern Australia: Australian Journal of Earth Sciences, **46**, 813-825.

Hunt, J.W., and A.T. Brakel, 1989, Relationship between geological setting and coal-type and quality in the Permian Basins, *in* Permian Coals of Eastern Australia: Bureau of Mineral Resources Bulletin, **231**,301-332.

Jahediesfanjani, H., and F. Civan, 2005, Damage tolerance of well-completion and stimulation techniques in coalbed methane reservoirs: Journal of Energy Resources Technology, **127**, 248-256.

Johnson, R.L. Jr., T. Flottman, and D.J. Campagna, 2002, Improving Results of Coalbed Methane Development Strategies by Integrating Geomechanics and Hydraulic Fracturing Technologies: Presented at the SPE Asia Pacific Oil and Gas Conference and Exhibition.

Kaiser, W.R., A.R. Scott, and R. Tyler, 1995, Geology and hydrology of coalbed methane producibility in the United States: Analogs for the world: Tuscaloosa, AL, Intergas Short Course.

Kalkomey, C., 1997, Potential risks when using seismic attributes as predictors of reservoir properties: The Leading Edge, **16**, 247-251.

Korsch, R.J., 2004, A Permian-Triassic retroforeland thrust system - The New England orogen and adjacent sedimentary basins, eastern Australia, *in* K.R. McClay, ed.,Thrust tectonics and hydrocarbon systems: AAPG Memoir, **82**, 515-537.

Lancaster, S., and D. Whitcombe, 2000, Fast-track 'coloured' inversion: 70th Annual International Meeting, SEG, Expanded Abstracts, 1-4.

Lisle, R.J., 1994, Detection of zones of abnormal strains in structures using Gaussian curvature analysis: AAPG Bulletin, **78**, 1811-1819.

Lynn, H., 2004, The winds of change: Anisotropic rocks-their preferred direction of fluid flow and their associated seismic signatures-Part 2: The Leading Edge, **23**,1258-1268.

Lynn, H., and W. Lynn, 2008, Using seismic attributes to characterize reservoir potential, plumbing, and risk for unconventional reservoirs: presented at the SEG Unconventional Resources Workshop in Vancouver.

Mai, H.T., 2010, Personal Correspondence at the University of Oklahoma, Spring 2010.

Mai, H.T., K.J. Marfurt, and S. Chavez-Perez, 2009, Coherence and volumetric curvatures and their spatial relationship to faults and folds, an example from Chicontepec basin, Mexico: 78th Annual International Meeting, SEG, Expanded Abstracts, 1063-1067.

Marfurt, K.J., and R.L. Kirlin, 2001, Narrow-band spectral analysis and thin-bed tuning: Geophysics, **66**, 1274-1283.

Marfurt, K.J., and H.T. Mai, 2009, Running AASPI Software with GUIs: University of Oklahoma.

Marfurt, K.J., 2010, Personal Correspondence at the University of Oklahoma, Spring 2010.

Marroquin, I.D., and B.S. Hart, 2004, Seismic attribute-based characterization of coalbed methane reservoirs: An example from the Fruitland Formation, San Juan basin,New Mexico: AAPG Bulletin, **88**, 1603-1621.

Mavor, M.J., and C.R. Nelson, 1997, Coalbed reservoir gas-in-place analysis: Gas Research Institute, 2-1.

McCrank,J., and D.C. Lawton, 2009, Seismic characterization of a CO_2 flood in the Ardley coals, Alberta, Canada: The Leading Edge, **28**, 820-825.

Mitra, S., 1990, Fault-Propagation Folds: Geometry, Kinematic Evolution, and Hydrocarbon Traps: AAPG Bulletin, **74**, 921-945.

Murray, G.H. Jr., 1968, Quantitative Fracture Study-Sanish Pool, McKenzie County, North Dakota: AAPG Bulletin, **52**, 57-65.

Nelson, R.A., 2001, Geologic Analysis of Naturally Fractured Reservoirs, 2nd Edition: Gulf Professional Publishing.

Ostler, S., 2002, Consultant Well Completion Report, 16.

Partyka, G., J. Gridley, and J. Lopez, 1999, Interpretational applications of spectral decomposition in reservoir characterization: The Leading Edge, **18**, 353-360.

Pattison, C.I., C.R. Fielding, R.H. McWatters, and L.H. Hamilton,1996, Nature and origin of fractures in Permian coals from the Bowen Basin, Queensland, Australia, *in* R. Gayer and I. Harris, eds., Coalbed Methane and Coal Geology: The Geological Society of London Special Publication, **109**, 133-150.

Pramanik, A.G., V. Singh, V. Rajiv, A.K. Srivastava, and D.N. Tiwary, 2004, Estimation of effective porosity using geostatistics and multiattribute transforms: A case study: Geophysics, **69**, 352-372.

Rai, C., 2009, Lab Observations Lecture: presented at the University of Oklahoma, Fall 2009.

Ramos, A.C.B. and T.L. Davis, 1997, 3-D AVO analysis and modeling applied to fracture detection in coalbed methane reservoirs: Geophysics, **62**, 1683-1695.

Roberts, A., 2001, Curvature attributes and their application to 3D interpreted horizons: First Break, **19.2**, 85-100.

Schraufnagel, R.A., 1993, Coalbed methane production, *in* B.E. Law and D.D. Rice, eds., AAPG Studies in Geology, **38**, 341-359.

Scott, A.R., 2000, Application of a coalbed methane producibility model to coalbed methane exploration, *in* C.E. Barker, A.R. Scott, and R.A. Downey, Coalbed Methane: From Prospect to Production Short Course: Opportunities in Alaska Coalbed Methane Workshop.

Scott, A.R., 2002, Hydrogeologic factors affecting gas content distribution in coal beds: International Journal of Coal Geology, **50**, 363-387.

Slatt, R.M., 2006, Stratigraphic Reservoir Characterization for Petroleum Geologists, Geophysicists and Engineers: Elsevier B.V.

Solano-Acosta, W., M. Mastalerz, and A. Schimmelmann, 2007, Cleats and their relation to geologic lineaments and coalbed methane potential in Pennsylvanian coals in Indiana: International Journal of Coal Geology, **73**, 219-236.

Suppe, J., 1985, Principles of Structural Geology: Prentice-Hall, Inc.

Taylor, G.H., M. Teichmuller, A. Davis, C.F.K. Diessel, R. Littke, and P. Robert, 1998, Organic Petrology: Berlin & Stuttgart, Gerbruder Borntraeger.

United States Geological Survey Website, 2010, http://vulcan.wr.usgs.gov/Imgs/Gif/PlateTectonics/Maps/map_plate_tectonics_world_bw.gif , accessed 28 March 2010.

Yee, D., J.P. Seidle, and W.B. Hanson, 1993, Gas sorption on coal and measurement of gas content, *in* B.E. Law and D.D. Rice, eds., AAPG Studies in Geology, **38**, 203-218.